

CHARACTERIZATION OF SELF-ASSEMBLED MONOLAYERS FOR USE AS A
MATRIX IN LASER DESORPTION IONIZATION

THESIS

Presented to the Graduate Council of
Texas State University-San Marcos
in Partial Fulfillment
of the Requirements

for the Degree

Master of SCIENCE

by

Kevin L. Francis, B.A.

San Marcos, Texas
August 2007

CHARACTERIZATION OF SELF-ASSEMBLED MONOLAYERS FOR USE AS A
MATRIX IN LASER DESORPTION IONIZATION

Committee Members Approved:

Walter Rudzinski, Chair

Chang Ji

Wendi David

Approved:

J. Michael Willoughby
Dean of the Graduate College

COPYRIGHT

by

Kevin L. Francis

2007

ACKNOWLEDGEMENTS

I would like to thank Dr. Walter Rudzinski for providing the opportunity to research self-assembled monolayers and helping me expand my analytical chemistry knowledge. His insights and direction have been crucial in the conception, approach and achievement of the thesis work presented here. Dr. Wendi David and Dr. Chang Ji deserve recognition for their instruction with instrumentation in their lab, surface plasmon resonance and electrochemistry set-up, in addition to serving on my thesis committee.

Several other members of the chemistry and biochemistry department deserve recognition for their time, guidance and permitting me access to their laboratory. Dr. Kevin Lewis proved insightful and eager to help on the development of a gel electrophoresis experiment with colloidal gold in his lab. Guidance on proton nuclear magnetic resonance and infrared spectroscopy were given by Dr. Michael Blanda. Instruction on molecular modeling and the opportunity to make atomic force microscopy measurements were provided by Dr. Gary Beal. Dr. Rachel Booth should also be recognized for allowing me access to her lab. MALDI experiments performed by the Rudzinski group were made possible by Dr. Ronald Walter.

As a general acknowledgement, I would like to thank the chemistry department at Texas State University-San Marcos for creating an open environment not only conducive to learning but courteous and professional.

This manuscript was submitted on August 1, 2007.

TABLE OF CONTENTS

	Page
ACKNOWLEDGEMENTS	iv
LIST OF TABLES	vii
LIST OF FIGURES	viii
CHAPTER	
1.0 INTRODUCTION AND BACKGROUND	1
1.1.0 The Problem.....	1
1.2.0 Background.....	2
1.2.1 MALDI-TOF of Oligonucleotides.....	2
1.2.2 Self-Assembled Monolayers.....	3
1.3.0 Preparation of SAMS.....	6
1.3.1 Formation of an Amine Reactive SAM	6
1.3.2 Immobilization of the Matrix.....	9
1.3.3 Immobilization of Polythymidylic Acid and Hybridization with Polyadenylic Acid	10
1.4.0 Significance of the Problem.....	11
2.0 EXPERIMENTAL.....	13
2.1.0 Substrate Utilized for the Creation of a SAM.....	13
2.1.1 Colloidal Gold.....	13
2.1.2 Vapor Deposited Au (1,1,1).....	14
2.2.0 Analytical Methods for Characterization of a SAM	15
2.2.1 Molecular Modeling.....	15
2.2.2 Atomic Force Microscopy	17
2.2.3 Infrared Spectroscopy	19
2.2.4 ¹ H Nuclear Magnetic Resonance	20
2.2.5 UV-Vis Absorbance.....	21
2.2.6 Gel Electrophoresis.....	23
2.2.7 Microgravimetry by Quartz Crystal Microbalance.....	24
2.2.8 Electrochemistry	26
2.2.9 Surface Plasmon Resonance	28
2.2.10 MALDI-TOF Mass Spectrometry.....	30

3.0 RESULTS	33
3.1.0 Analytical Methods.....	33
3.1.1 Molecular Modeling.....	33
3.1.2 Atomic Force Microscopy	41
3.1.3 Infrared Spectroscopy	44
3.1.4 ¹ H Nuclear Magnetic Resonance	46
3.1.5 UV-Vis Absorbance.....	48
3.1.6 Gel Electrophoresis.....	52
3.1.7 Microgravimetry by Quartz Crystal Microbalance.....	57
3.1.8 Electrochemistry	61
3.1.9 Surface Plasmon Resonance	68
3.2.0 MALDI-TOF Mass Spectrometry.....	72
4.0 Conclusions.....	77
4.1.0 Discussion of Analytical Results	77
REFERENCES	80

LIST OF TABLES

Table	Page
2-1. MALDI Experiment 1	31
2-2. MALDI Experiment 2	31
2-3. MALDI Experiment 3	32

LIST OF FIGURES

Figure	Page
1-1. Possible Reactions with DSP.....	7
1-2. Examples of Immobilized Matrix.....	9
1-3. SAM of DSP-Matrix.....	10
2-1. Micrograph of AFM Sample	18
2-2. QCM Instrument.....	25
3-1. Lying Down Phase of SAM.....	34
3-2. Upright Phase of SAM	35
3-3. Surface Angle of DSP.....	36
3-4. Height of DSP Monolayer	37
3-5. Spacing of DSP Monolayer	38
3-6. Orientation of Immobilized Oligomer	40
3-7. AFM Measurement of Au.....	42
3-8. AFM Measurement of Au-DSP	42
3-9. AFM Measurement of Au-DSP-Matrix.....	43
3-10. AFM Measurement of Au-DSP-dT ₂₀	44
3-11. IR Spectra of DSP and Tryptamine	45
3-12. IR Spectra of Conjugate	46
3-13. ¹ H NMR Spectra of Au-DSP-Matrix.....	47
3-14. UV-Vis Absorbance Spectra of Au-DSP.....	49

3-15. Phase Transition of Functionalized Colloidal Gold	51
3-16. UV-Vis Absorbance Spectra of Colloidal Gold Samples.....	52
3-17. Gel Electrophoresis of Low Concentration Colloidal Gold Samples.....	53
3-18. Fluorescence Image of Low Concentration Colloidal Gold Samples	54
3-19. Gel Electrophoresis of High Concentration Colloidal Gold Samples	56
3-20. Fluorescence Image of High Concentration Colloidal Gold Samples.....	57
3-21. QCM Plot of Au-DSP	58
3-22. QCM Plot of Au-DSP-Matrix.....	59
3-23. QCM Plot of Au-DSP-dT ₂₀	61
3-24. Voltammogram of Au-DSP	62
3-25. Voltammogram of Au-DSP-Matrix	63
3-26. Voltammogram of Au-DSP-dT ₂₀	64
3-27. CV of Gold Electrode	65
3-28. CV of Au-DSP	66
3-29. CV of Au-DSP-Matrix.....	67
3-30. CV of Au-DSP-dT ₂₀ and Au-dT ₂₀	68
3-31. SPR Plot of Au-DSP-dT ₂₀	69
3-32. SPR Plot of Au-DSP-Matrix.....	70
3-33. SPR Plot of Au-DSP-dT ₂₀ -dA ₂₀	72
3-34. MALDI Spectra of Au	73
3-35. MALDI Spectra of Au-DSP-Matrix	75
3-36. MALDI Spectra of Mixed SAM.....	76

CHAPTER 1.0

INTRODUCTION AND BACKGROUND

1.1.0 The Problem

The analysis of inherently low concentrations of biomolecules in microvolume sized samples has been a continuing challenge. Analytical techniques such as matrix assisted laser desorption ionization (MALDI) have provided the much needed sensitivity and rapid sample processing for such demanding biological samples. The technique involves encasing a sample within a crystalline matrix support that is capable of transferring laser energy such that ionization and desorption of the analyte can occur. However, this technique isn't without its pitfalls. Matrix tends to add significantly to the background in the mass range below 1000 m/z. The inhomogeneous and variable nature of the matrix complicates a true understanding of the mechanism by which matrix functions making correction of the background difficult. One goal of the research presented is to produce a MALDI sample that doesn't involve creating an inhomogeneous, crystalline matrix it might be possible to minimize matrix induced interferences in the low mass range and possibly elucidate the role of matrix.

MALDI requires sample processing to remove excess salts and separation of the desired analyte. Through immobilized affinity chromatography (IAC) sample clean-up and isolation has generated a desirable sample for MALDI analysis.¹⁻³ This

chromatographic technique provides specific isolation of a species through biological interactions (such as antibody/antigen, enzyme/substrate, oligomer/compliment) by affixing half of the pair to the chromatographic support. For low concentration samples or those that display a high binding coefficient, analytes can be lost to the clean-up procedure of IAC. A second research goal is to minimize the sample loss observed in IAC putting less emphasis on the sensitivity of MALDI.

1.2.0 Background

1.2.1 MALDI-TOF of Oligonucleotides

Since its relatively recent inception in 1988, Matrix Assisted Laser Desorption Ionization (MALDI) has been an indispensable tool for the analysis of oligonucleotides and proteins. MALDI, as an ionization source for mass spectrometry, is attractive for large biomolecules because it generates high yields of the molecular ion peak allowing sub-picomole sensitivity.⁴ While molecules up to 300 kDa are well within the capabilities of MALDI, those below 1000 Da aren't routinely analyzed by MALDI given the high background generated by the matrix. The ions have little excess energy and demonstrate minimal propensity to fragment which facilitates the analysis of multi-analyte samples. The mass accuracy is lower when used with time of flight (TOF-MS) but high resolution can be obtained with Fourier transform (FT-MS).⁵ MALDI suffers from background interference from the matrix and matrix adduction but the role of matrix is crucial to generating the molecular ion.

A common method of sample preparation involves mixing analyte in a solution of excess matrix and subsequently drying on a MALDI plate. Once dried, the matrix forms a crystal matrix encasing and isolating the analyte. Applying a pulsed laser beam to the

crystal matrix creates rapid heating sufficient enough for sublimation of the analyte encased in matrix. The exact mechanism of desorption and subsequent ionization of the analyte is still under evaluation, but a few theories have been formed.

One such theory is the thermal-spike model which suggests that the matrix and analyte demonstrate negligible vibrational coupling which would permit vibrational energy transfer from matrix to analyte.⁴ A second theory, the pressure pulse theory, suggests that a force normal to the plate is generated by the high energy matrix. Analytes are expelled by a transfer of momentum from the matrix and ionized by proton transfer. Complicating the elucidation of the role of matrix in MALDI is the inhomogeneous crystalline complex formed by the matrix and analyte. The resulting crystals formed after evaporation of solvent vary in size and shape. This irregularity leads to spot variations in analyte concentration which generates inconsistencies in signal intensity and complicates efforts to understand the ionization mechanism performed by matrix of MALDI.⁴

1.2.2 Self-Assembled Monolayers

Within the past few decades it has become increasingly common knowledge that properties of compounds confined to a surface are significantly different from that in bulk. The properties of molecules at the surface have been largely ignored in the past because they contributed but a negligible effect on the overall properties of the bulk. However, in the passing few decades science has moved into the exploration of micro and even nano domains where surface interactions play a significant role in determining the properties of nanoparticles. Chemistries based on colloid solutions, emulsions, corrosion, and detergency are but a few examples of the change in focus. Analytical instrumentation has also moved into the nano environment with surface plasmon

resonance, atomic force microscopy and microgravimetry with a quartz crystal microbalance to help gain an understanding of the near atomic environment. All of the aforementioned instances involve the adsorption of molecules in solution to a solid substrate so a thorough understanding of this mechanism is of great importance.

Adsorption onto a surface is an entropy driven process resulting in an ordered array. Molecules are evenly spaced in a uniform monolayer based on their coordination with the surface and intramolecular forces which give rise to the term self-assembled monolayer or SAM as it will be referenced. The adsorption of molecules to a surface, such as in the formation of a SAM, is achieved by two mechanisms that are nearly indistinguishable. The two mechanisms of physisorption and chemisorption that are crucial to the formation of a self-assembled monolayer will be outlined below.

Physisorption is the longer in range of the two mechanisms encompassing van der Waals interactions between the substrate and the adsorbate (species being adsorbed to the surface). The interaction is driven by the favorable potential energy of the system where the forces become exponentially stronger as the distance between adsorbate and surface decrease. It's easy to envision the attraction between two species of opposing electric dipoles, but physisorption also involves non-polar attractions. Physisorption forces can be aided by the hydrophobic effect for molecules that display a negative change in entropy with the addition to an aqueous solution. The hydrophobic effect can be best thought of as a tendency for greater disorder of the solvent with precipitation of the non-polar species. If an adsorbate is nonpolar in nature then it will be driven to a nonpolar surface in an aqueous medium. As the molecule condenses on the surface there is a release of energy (enthalpy of condensation) that is converted into vibrational motion

along the surface. Vibrational energy is lost to the environment as thermal energy and the molecule becomes immobilized.⁶⁻⁸

Typical chemisorption involves the formation of a covalent bond with the substrate that follows coordination chemistry. Values for the enthalpy of chemisorption are an order of magnitude greater than what is observed for physisorption making it a more desirable route to immobilization. While this mechanism produces a strong interaction between adsorbate and substrate, an adsorbed molecule can be torn apart if there are unsatisfied valencies in the substrate.⁶⁻⁸

One way to define adsorption mathematically is through the Langmuir adsorption isotherm.^{9, 10} The relation has many restrictions but it still proves adequate even when these restrictions are not met. The equation relates the surface concentration of a species (C) to the concentration of a monolayer of the species (C_{SAM}) and the concentration of the species in solution (C_{sol}).

$$C = \frac{C_{SAM} C_{sol}}{C_{sol} + (55.5 \exp(\Delta G^\circ / RT))}$$

The conditions under which this equation is viable are: the adsorbent is homogeneous, both solute and solvent have equal molar surface areas, both surface and bulk phases do not interact and the adsorption film is monomolecular.^{7, 8, 11}

A typical model for a SAM is alkyl thiols that readily form a monolayer on a gold substrate.^{12, 13, 14} The thiol end of the molecule chemisorbs to a gold surface creating a gold thiol bond (RS-Au). There is still some debate as to whether the proton originally attached to the thiol dissociates with the formation of the gold to thiol bond to form hydrogen gas, or remains attached to the alkyl thiol.^{15, 16} The initial molecules bound to

the surface adopt a “lying down” phase where the hydrophobic tails orient parallel to the surface due to the hydrophobic effect. As the gold substrate continues to populate with alkyl thiols, van der Waals forces between alkyl chains start to influence the structure. With the increasing density of alkyl thiols on the surface, the chains transition into an upright geometry typically adopting an angle 30° from the surface normal.¹⁶⁻¹⁸

Deposition of the adsorbate is on the order of minutes for concentrations of 1-10 mM but the formation of an ordered array can take several days. Interactions between adsorbed molecules create a highly ordered array on the gold surface.¹²

SAMs have seen many applications in chemical sensors.¹⁹⁻²⁶ Through the use of a SAM it will be possible to immobilize a probe oligomer and matrix for MALDI analysis.

1.3.0 Preparation of SAMS

1.3.1 Formation of an Amine Reactive SAM

Many discussions that revolve around SAMs on a gold substrate involve taking the desired adsorbate and adding a thiol group, if not preexisting.^{13, 14, 27, 28} While an effective route to creating a SAM, the process of labeling with a thiol is laborious. The use of an appropriate coupling reagent bypasses the organic synthesis process to yield a similar result.

Immobilization of oligomers and matrix may be done through the homobifunctional crosslinker dithiobis(succinimidylpropionate) hereafter referred to as DSP. The bisymmetrical DSP may link to ϵ -amine groups on the α -amine position of N-terminal amino acids.^{1, 29} The cross-linker has also found applications outside of protein chemistry for the immobilization of species containing primary amines to a gold surface.^{19, 20, 22, 24, 30} The succinimidyl ester (NHS) of DSP is an ideal leaving group to

electron donating primary amines. Attack occurs at the electron deficient carbon of the ester on DSP by a primary amine to create an amide bond (Figure 1-1). Hydrolysis of DSP to the carboxylate is an unwanted side reaction that can be controlled by optimizing pH to conditions, typically in the range of 7.0-9.0, favoring the amide reaction.

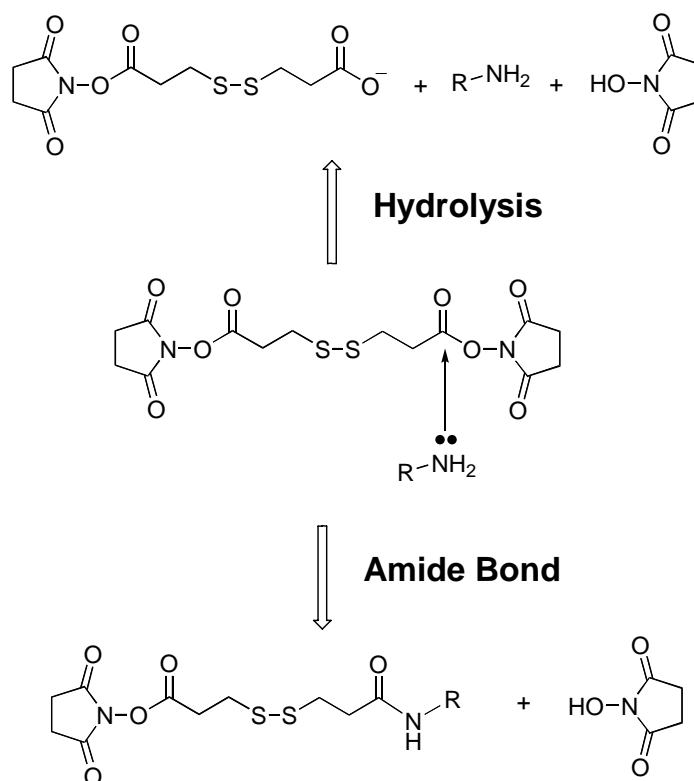


Figure 1-1. Possible Reactions with DSP. Reaction of DSP with a primary amine containing species outlining possibilities of the formation of an amide bond or hydrolysis.

With the growing use of DSP several analogs have developed. One such compound is dithiobis(sulfosuccinimidyl propionate) (DTSSP) which is water soluble, unlike DSP, thanks to a sulfate group on NHS.³¹⁻³⁴ Yet another analog of DSP that has found use is dithiobis(succinimidyl undeconate) (DSU) which pushes the linked species farther apart thanks to an eleven carbon spacer.^{22, 30, 35-38} An eleven carbon spacer may demonstrate greater stability and higher order in a SAM than shorter spacer arms.^{39, 40}

As outlined, DSP provides a pathway to cross-linking through its NHS groups and a second feature of immobilization with the disulfide group. Hermanson has suggested cleavage of the disulfide bridge with the reducing agent dl-dithiothreitol (DTT) to facilitate attachment to a gold surface but, this has been demonstrated to be an unnecessary step in achieving immobilization.^{1, 15, 20, 22, 30} In either case, the covalent bond between gold and the thiol is fairly robust with a binding energy in the neighborhood of 100 kJ/mol.

Protocols for attaching primary amine containing species to a gold substrate by means of DSP can take roughly two approaches. Both procedures share the first step of dissolving DSP in an organic solvent, typically DMSO or DMF which can then be diluted in an aqueous medium, to a concentration of 10-25 mM. An aliquot of this solution can be added to a gold substrate, where DSP forms a SAM, or to a primary amine containing solution to form the crosslinked species. Manufacturer suggestions are to add excess molar amounts of DSP (exact ratios are dependant on the concentration of the species to be cross-linked) due to the competing reaction of hydrolysis. Creating a monolayer of DSP first offers the advantages of stability to hydrolysis, and minimal use of immobilized species.^{24, 30} Wagner has claimed activity of a DSP coated surface after 37 hours at pH 8.5, which is far more attractive than a half life of thirty minutes for DSP in solution.³⁰ The final step is to either react the DSP coated surface with the primary amine or immobilize the DSP-amine conjugate to the gold substrate.³ The creation of a monolayer of DSP followed by conjugation was the method chosen for the creation of a SAM in this work. Through this mechanism, the immobilization of oligomer probes and matrix to gold will be explored.

1.3.2 Immobilization of the Matrix

Matrix functions as a protonation/deprotonation source and absorbs the brunt of incident UV laser radiation and transfers this energy towards ionization of the analyte. The selection of a matrix compound is a function of the laser used and the class of compound under examination. The matrix should exhibit strong absorbance at the laser wavelength, with low enough mass to sublime and still be relatively inert. Although many compounds have been screened as possible matrices, relatively few compounds have proven useful.^{41, 42}

The idea to explore the use of *n*-*boc*-1,4-phenylene diamine as a matrix comes from the literature.⁴² Smith et al. demonstrated success with the compound methyl *n*-(4-mercaptophenyl) carbamate (MMPC) as a SAM of matrix which spurred the Rudzinski group to follow suit with an analog of MMPC under slightly different conditions (Figure 1-2). The Smith group chose to immobilize matrix directly to the surface while the attempt here is to use DSP as an intermediate to achieve immobilization.

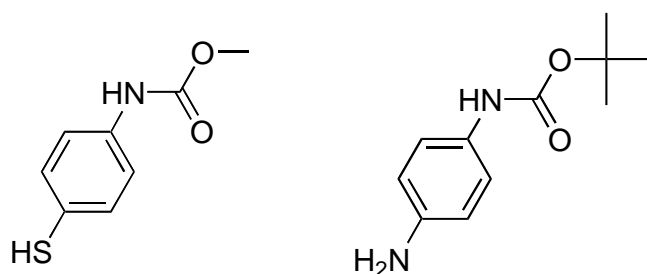


Figure 1-2. Examples of Immobilized Matrix. Comparison of matrix used by Smith group (MMPC) to the compound *n*-*boc*-1,4-phenylene diamine under evaluation.

The addition of *n*-*boc*-1,4-phenylene diamine to a substrate through the crosslinker DSP was approached by variations on two attachment schemes. Both of these processes share the same ultimate goal of utilizing *n*-*boc*-1,4-phenylene diamine as a matrix in intimate contact with the oligonucleotide duplex. In one scenario duplex was

immobilized onto a colloidal gold substrate by means of DSP and mixed with gold nanoparticles functionalized with matrix. A second approach was to immobilize matrix on the same substrate as the duplex in a mixed SAM. If the duplex adopted a lying down phase it would be in intimate contact with neighboring matrix molecules. For the case of an upright phase of oligomer, it is thought that the first scenario would be a better application of matrix. Variations on these basic schemes were approached experimentally. A stylized representation of the reaction between DSP and *n*-*boc*-1,4-phenylene diamine is given in Figure 1-3.

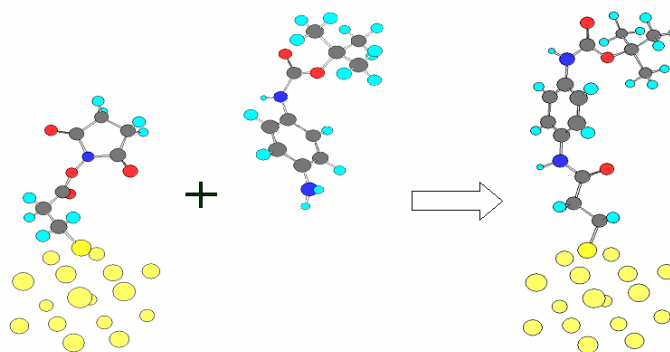


Figure 1-3. SAM of DSP-Matrix. Reaction of DSP immobilized on gold with the matrix (*n*-*boc*-1,4-phenylene diamine) under evaluation.

1.3.3 Immobilization of Polythymidylic Acid and Hybridization with Polyadenylic Acid

Oligonucleotides are single stranded nucleic acid polymers typically consisting of fifty or fewer bases. Used as a probe, oligonucleotides are capable of highly selective detection through exclusive binding with the complementary base sequence. Binding of moieties to oligomers occurs at the 5' or 3' end of the polymeric chain or with insertion.^{43, 44}

Immobilization of an oligomer to a DSP coated surface will be made possible by labeling the 5' end with a six carbon spacer arm (C6) to which a primary amine will be

tethered. The C6 spacer arm ensures that the primary amine is not sterically hindered and can form an amide bond with DSP. Reaction conditions of pH 7-9 and salt concentrations will reflect manufacturer's recommendations but more time will be allotted for the reaction to occur due to the slower diffusion rate of an oligonucleotide.

With the polythymidylic acid (dT₂₀) probe immobilized to the surface a known concentration of polyadenylic acid (dA₂₀), typically ten times the concentration of dT₂₀, will be added maintaining buffer conditions and allowing hybridization with the immobilized dT₂₀. Normally an annealing step is conducted to correct mismatched pairs with hybridization. The effectiveness of an annealing step between oligomers with identical bases was questioned and therefore not approached.

1.4.0 Significance of the Problem

There has been limited success in creating a more uniform analyte-matrix surface through vacuum drying, electrospray deposition, or spin coating. From the growing list of pathways to create a uniform analyte-matrix, the creation of a self-assembled monolayer (SAM) is of particular interest to the Rudzinski group. Self-assembled monolayers have demonstrated popularity in a variety of fields but only a few instances have appeared applying this strategy to a MALDI matrix.⁴²

By immobilizing the matrix to the MALDI plate, matrix molecules will be less likely to appear in the plume of ablated sample and contribute to background or adducts. Two different gold substrates, colloidal gold and gold plate, will be utilized to encourage intimate contact between matrix and analyte. Colloidal gold of its own accord will also be investigated as a matrix since it has displayed some success as a matrix.⁴⁵ It's also hoped that by performing sample isolation and clean-up on the MALDI plate through the

creation of a highly selective SAM, in place of IAC, sample processing will ultimately be improved.

CHAPTER 2.0

EXPERIMENTAL

2.1.0 Substrate Utilized for the Creation of a SAM

2.1.1 Colloidal Gold

The use of colloidal gold offers a far greater surface area than what's available from planar electrodes. Another advantage offered by gold nanoparticles is the increase in binding kinetics which is a function of the greatly reduced diffusion distances.

One approach to determining the number of gold nanoparticles in solution utilizes absorbance around 520 nm attributed to surface plasmon resonance. As Cumberland and Strouse demonstrated, Beer's law ($A = \epsilon bc$) allows a direct spectrometric determination of concentration (c) given the molar extinction coefficient (ϵ) for Au-Cl of $9.93 \pm 0.48 \times 10^6 \text{ M}^{-1} \text{ cm}^{-1}$.⁴⁶ An average absorbance measurement (A) colloidal gold of path length (b) 0.71 cm gives 0.52 ± 0.08 . The count determined by absorbance measurements is 98% of the manufacturers (Aldrich; St. Louis, MO) stated absorbance ($A = 0.75$ for $b = 1$) so the actual concentration of HAuCl_4 is 0.0098% of gold nanoparticles.

The available surface area of colloidal gold was then estimated. Starting with the measured value of 0.0098% HAuCl_4 would mean that there is 0.0579 mg of gold in one milliliter of solution ($196.97/339.78 = 0.579$). Since the diameter of the colloidal

particles is 10 ± 2 nm it is possible to determine the area and volume ($A = 4\pi r^2$, $V = 1.33\pi r^3$) of a single particle assuming a spherical shape.⁶⁸

$$A = 4 \times \pi \times 5^2 = 314nm^2$$

$$V = 1.33 \times \pi \times 5^3 = 524nm^3$$

Knowing the density of gold to be 19.3 g/mL then the number of gold nanoparticles and total surface area can be determined.

$$V_{Au} = \frac{0.057g}{mL} \left(\frac{1g}{1000mg} \right) \left(\frac{mL}{19.3g} \right) = 3 \times 10^{-6}$$

$$nanoparticles / mL = \frac{nanoparticle}{524nm^3} \left(\frac{1 \times 10^7 nm}{cm} \right)^3 3.0 \times 10^{-6} = 5.7 \times 10^{12}$$

$$mm^2 / mL = 314nm^2 \left(\frac{mm}{1 \times 10^6 nm} \right)^2 5.7 \times 10^{12} = 1.8 \times 10^3$$

Colloidal gold was applied in the surface characterization experiments of atomic force microscopy (AFM), proton NMR, UV-Vis absorption, and gel electrophoresis. Its ultimate role was to not only serve as a substrate for the immobilization of matrix and oligomer but also as a laser desorption ionization source.

2.1.2 Vapor Deposited Au (1,1,1)

Vapor deposited gold surfaces were incorporated into various sensor designs allowing a direct measurement of the SAM. Typical fabrication of a vapor deposited gold surface consists of applying an intermediate binding layer such as titanium or chromium, 50 to 200 Å in thickness, to a glass or quartz surface before depositing a layer of gold. These surfaces are taken to be the Au (1,1,1) plane which offers the tightest arrangement of atoms in a cubic close packed (ccp) crystal structure.

Three different analytical procedures employed the use of a vapor deposited gold surface. Quartz crystal microbalance (QCM) is the first analytical method discussed which uses 100Å of Ti as a binding layer for 1000Å of Au on a quartz crystal (CH Instruments; Austin, TX). For electrochemistry experiments a Ti/Au coating was applied to a 1''×0.25''×0.04'' borofloat glass substrate (EMF Corporation; Ithaca, NY) which could be clipped and utilized as a working electrode. Surface plasmon resonance (SPR) employed an instrument specific gold coated sensor chip (GE Healthcare Biacore AB; Sweden).

2.2.0 Analytical Methods for Characterization of a SAM

2.2.1 Molecular Modeling

A Silicon Graphics Octane computer loaded with Cerius 2, (revision 00.0222) and MatSci (version 4.2.) was used for molecular modeling to predict the behavior of the self-assembled layer of DSP on a gold surface. Parameters of the software were left in their default configurations unless otherwise noted. A description of how the self assembled monolayer was stylized is described in the following paragraphs.

The first step in defining the SAM by molecular modeling was to create the Au (1,1,1) surface. This was done by picking the appropriate space group of face centered cubic (fcc) or Fm-3m as labeled by Cerius², the cell spacing of 407.82 pm, and gold as the atom to be arranged in the crystal lattice. A 10×10×10 nm cube of (fcc) gold was created so that a (1,1,1) face could be generated by removing atoms above the defined plane (The selection of the close packed surface (1,1,1) to construct a SAM was chosen since this is a common surface to QCM and SPR sensor surfaces). As a final step, the gold layer is constrained to prevent unnatural migration of the atoms as a result of

subsequent modeling. The Au (1,1,1) surface needs no further attention beyond the aforementioned steps therefore, building a molecular representation of DSP and mimicking the deposition of DSP are the next focus.

The DSP molecule is produced by crudely arranging the appropriate atoms, loading a force field (universal 1.02) and applying charges to the atoms of the molecule. With the charges applied, the structure can be realized by performing energy minimization and subsequent dynamics simulations steps. Energy minimization and dynamics calculations are performed multiple times with manual displacement of atoms or increasing the displacement force between steps to ensure a representative structure of the molecule.

To simulate chemisorption and van der Waals interactions between DSP and the Au (1,1,1) surface only half of the bisymmetrical molecule DSP was utilized. Adsorption of DSP from solution and breaking of the disulfide bond will be inferred steps in the creation of a SAM.^{1, 15, 20, 22, 30} The deposition of the first DSP fragment was as simple as creating a bond between sulfur and one of the centrally located gold atoms on the Au (1,1,1) surface. A second DSP fragment was brought into proximity of the first immobilized fragment such that the succinimidyl endgroups of the two molecules were farthest apart and the thiol groups were the closest atoms between the two molecules. This orientation was chosen to mimic the steps of physisorption and/or chemisorption of an intact DSP molecule leading to cleavage of the disulfide bond and deposition of the identical DSP fragments. The attachment site of a second DSP fragment to the gold surface was chosen based on the closest allowable site as determined by numerous iterations of energy minimization and dynamics simulations. Population of the surface

with DSP fragments continued outward from these initial fragments until realizing a SAM of DSP. The most likely arrangement of DSP molecules on the surface was determined as that which generated the lowest sum of kinetic and potential energy of the system.

With an optimal configuration of a monolayer of DSP, interactions of immobilized oligomer with the SAM were studied. In a similar fashion to creating a model of DSP, the construction of a molecular representation of an oligomer consisting of twenty polythymine (dT₂₀) was achieved by arranging the appropriate atoms, loading a force field (universal 1.02) and applying charges to the atoms of the molecule. A model of the dT₂₀ oligonucleotide bound to the DSP surface through an amide bond on the end of a C6 spacer arm was generated. Interactions between the surface and the oligonucleotide were studied.

2.2.2 Atomic Force Microscopy

With atomic force microscopy (AFM) a sharp stylus attached to a cantilever beam is maneuvered across a smooth surface. Any force that acts on the stylus bends the cantilever beam. A laser reflected off of the tip of the cantilever determines the distance, or height, of the beam deflection. By raster scanning a surface area, objects that are nanometers in size can be imaged through AFM.^{6, 7}

The instrument utilized for AFM measurements was a Veeco Dimension 3100 AFM from Veeco Metrology (Santa Barbara, CA) located in the Physics department of Texas State. The spin coater used in applying the colloidal gold to the silicon substrate was a Laurell (North Wales, PA), WS-400A-6NPP/Lite operated at 1000 rpm for 1 min then ramped to 1500 rpm for 20 seconds with a final step to 2000 rpm for 20 seconds.

Samples were prepared by cutting a silicon wafer into roughly 1"×1" pieces onto which 50 μL of a sample was deposited. The sample was then placed on the spin coater vacuum chuck and run through the program outlined above. A second application of 50 μL was performed as before to ensure deposition of the colloidal gold. The prepared samples were individually analyzed by securing them on the stage, and conducting contact-mode AFM. The tip was manually located and positioned within range of the substrate surface following mounting of the sample.

The wafer surface of the sample was visually scanned, aided by a Nanoscope Dimension 3100 Controller, to find dried droplets of sample for conducting AFM measurements. A typical spot is demonstrated in Figure 2-1.

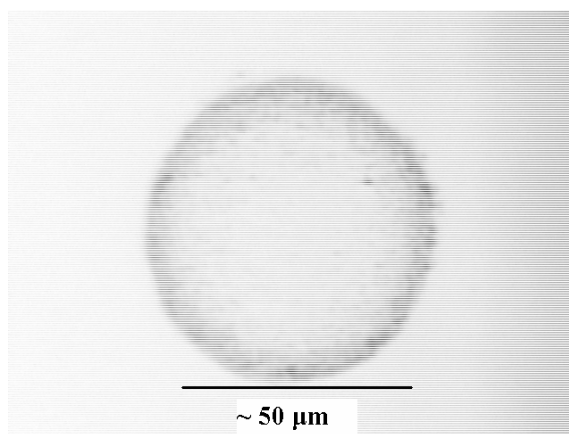


Figure 2-1. Micrograph of AFM Sample. Micrograph of a dried collection of colloidal gold found on the silicon surface.

Once a collection of dried colloidal gold particles was visually sighted, a 60 μm × 60 μm AFM measurement of the spot was performed followed by analysis on a tighter frame of 5 μm × 5 μm . AFM parameters were not modified between samples except those controlled by the instrument.

Colloidal gold samples for AFM analysis were prepared by adding 50 μL of 1 mM DSP to 1000 μL of colloidal gold suspension. This mixture was allowed to react for 30 minutes before performing a solvent exchange with a HEPES based buffer through centrifugation. The colloidal gold was suspended in 190 μL of a HEPES based buffer solution (1.19 g of HEPES (EM Science; Lawrence, KS), 1.64 g of NaCl (EM Science; Lawrence, KS), 0.021 g Na_2HPO_4 (J.T. Baker; Phillipsburg, NJ) in 100 mL of double distilled water) at pH 8.0 before adding 10 μL of either 10 mM of *n*-boc-1,4-phenylene diamine or 1 mM of dT_{20} and allowed to react overnight. A colloidal gold control and DSP labeled colloidal gold were prepared in tandem with the matrix and dT_{20} oligonucleotide samples.

2.2.3 Infrared Spectroscopy

Atoms held by covalent bonds are in continual vibrations, or oscillations, which can be altered by the absorption of a selective wavelength of infrared radiation. This absorption leads to an excited vibrational state and is specific to an atomic pair held in a bond. Each bond can undergo various oscillations resulting in the absorption of numerous wavelengths. These vibrations are classified as the fundamental modes and can be described as stretching and bending vibrations.⁴⁷ The degree of infrared energy absorption is related to the change in the bond moment which explains why non-polar bonds do not absorb infrared radiation.

A Perkin Elmer (Waltham, MA), Spectrum One was utilized for FT IR measurements performing ten scans at 4 cm^{-1} resolution. Infrared absorption was measured between $4000 - 800\text{ cm}^{-1}$. Spectra were interpreted through comparison of the

spectra with well developed spectral libraries in order to determine the nature of the bonds for the sample in question.

Ten milligrams of the reactant species, DSP (Pierce; Rockford, IL) and tryptamine (Aldrich; St. Louis, MO), were weighed out separately and dissolved in one milliliter of acetone (Sigma; St. Louis, MO). Several drops of the solution were placed on a polyethylene substrate and set aside for the acetone to evaporate. Once dried, the sample formed a thin film on the polyethylene which was analyzed.

Infrared measurements of the DSP-tryptamine conjugate were achieved by dissolving fifty milligrams of tryptamine and twenty milligrams of DSP in 100 μ L of dimethylformamide (Sigma; St. Louis, MO). This solution was dissolved in one milliliter of a HEPES based buffer at a pH of 8.0 and allowed to react for thirty minutes. The product resulted in a white precipitate that was separated by filtration and drying. The isolated powder was measured on the same Perkin Elmer, Spectrum One but this time with the attenuated total reflection (ATR) attachment.

2.2.4 ^1H Nuclear Magnetic Resonance

Nuclear Magnetic Resonance (NMR) monitors the absorption of radio frequency radiation in the presence of a magnetic field.⁵ Characteristic absorption is a property of the magnetic dipole of the nuclei. Spectra of nuclei, such as ^1H , are obtainable since they have spin numbers of $\frac{1}{2}$ and a uniform distribution of charge.⁵ In typical Fourier transform NMR, a sample is pulsed with a range of radio frequencies, exciting the nuclei in a sample and a detector collects the energy released as a function of time. The compiled energy signals from the free induction decay are transformed to a spectrum based on frequency.

^1H NMR spectra were obtained at 400 MHz with a Varian (Palo Alto, CA), Unity Inova equipped with an Oxford NMR 400 spectrometer. Samples were placed in a New Era (Vineland, NJ) NE-HL5-7" zirconia rotor with 0.5 mL of CDCl_3 as a solvent. Samples for ^1H NMR were prepared by reacting five milliliters of the colloidal gold solution with 250 μL of a 100 μM solution of DSP for 15 minutes. A solvent exchange was performed by spinning down the colloidal gold samples for 40 min and resuspending in 500 μL HEPES based buffer at pH 8.0. To this DSP functionalized gold solution 250 μL of a 500 μM solution of *n*-*boc*-1,4-phenylene diamine (Fluka) in dimethylformamide (Sigma-Aldrich; St. Louis, MO) was added and allowed to react for 15 minutes. The sample was spun down at 18,000 rcf on a Beckman Coulter (Fullerton, CA), Microfuge 18 centrifuge for 40 minutes and suspended in D_2O .

2.2.5 UV-Vis Absorbance

A UV-Vis absorption measurement outlines energy level separations for electronic transitions with superimposed vibrational and rotational transitions which together create a large absorption band.^{7, 48} Absorption spectroscopy then typically involves a sweep of monochromatic wavelengths over a range of frequencies generating a UV-Vis spectrum. Analyses were performed on a Molecular Devices (Sunnyvale, CA), Spectra Max190 plate reader.

Trying to decipher the presence of a large molecule by UV-Vis absorption alone is a daunting task considering there are so many overlapping transitions with broad peaks. However, gold offers a fairly unique transition around 520 nm attributed to surface plasmon resonance (SPR). The mechanism of SPR is covered in section 2.2.9 and will not be addressed here. With colloidal gold, absorption measurements in the range of 450-

650 nm can provide a quantitative measurement of both the amount and nature of surface interactions.

A colloidal gold solution consisting of 0.01% of HAuCl_4 of particle size 10 ± 2 nm, passivated by 0.01% tannic acid, 0.04% trisodium citrate and 0.26 mM potassium carbonate was obtained from Sigma (St. Louis, MO). Ten microliters of DSP (Pierce; Rockford, IL) at concentrations ranging from 100 nM to 1 mM, prepared at concentration increments of ten, were dissolved in dimethyl formamide (Sigma; St. Louis, MO) were added to a 100 μL of colloidal gold solution. The reaction between DSP and colloidal gold was allowed to proceed for 15 minutes before obtaining the spectrum.

A second UV-Vis experiment was performed to display activity of the SAM of DSP on gold. DSP was deposited on colloidal gold under conditions designed to prevent aggregation; namely, 10 μL of 100 μM DSP were added to 200 μL of colloidal gold, as determined previously. Functionalized colloidal gold solutions were centrifuged for 40 minutes following a 15 minute deposition step. Pelleted solutions were suspended in 200 μL of a HEPES based buffer solution (1.19 g of HEPES (EM Science; Lawerence, KS), 1.64 g of NaCl (EM Science; Lawerence, KS), 0.021 g Na_2HPO_4 (J.T. Baker; Phillipsburg, NJ) in 100 mL of double distilled water) at pH 8.0. To the buffered colloidal gold solutions containing DSP, 10 μL of 1000 μM dT_{20} was added and allowed to react overnight. Unreacted DSP sites on the colloidal gold were then capped with 50 μL of 4 mM of Tris(hydroxymethyl)aminomethane (Tris) supplied by RPI (Mt. Prospect, IL). The reaction between DSP and Tris was allowed to proceed for 45 minutes to ensure quenching of unreacted DSP.

2.2.6 Gel Electrophoresis

Electrophoresis is a technique based on the movement of charged molecules in the presence of an applied electric field. Separation is made possible based on differences in the ratio of charge to frictional coefficient. The frictional coefficient is a function of the hydrodynamic size and shape of a molecule. The use of support media, such as agarose, minimizes convection and diffusion that would otherwise interfere with the separation.⁴⁹

A 10× phosphate running buffer was prepared by weighing out: 1.09g NaHPO₄ (J.T. Baker; Phillipsburg, NJ) and 0.32 g NaH₂PO₄ (J.T. Baker; Phillipsburg, NJ) diluted to 100 mL with double distilled water. Agarose gels, OmniPur (EMD, Germany), were prepared at a 1.00% w/v in phosphate running buffer. Gels were loaded with twelve microliters of the concentrated sample along with 4 µL of 25% glycerine. A 50 base pair ladder was obtained from New England Biolabs (Ipswich, MA). A horizontal gel electrophoresis apparatus from Life Technologies (Gaithersburg, MD), Horizon 11 14 coupled to a power supply from E-C Apparatus Corporation (Boston, MA), EC-105 was used to run the agarose gels. The gel was run with a potential of 100 V for one hour before staining with ethidium bromide for 15 minutes. Fluorescence imaging was made possible with a Kodak Digital Science Image Station (Rochester, NY), 440 CF equipped with a #25 (523 nm) cut off high pass filter.

Gel electrophoresis was performed with colloidal gold particles to demonstrate binding of oligonucleotide to the gold surface. A colloidal gold solution prepared from a 0.01% solution of HAuCl₄ (particle size 10 ±2 nm), passivated by 0.01% tannic acid, 0.04% trisodium citrate and 0.26 mM potassium carbonate was used.

The colloidal gold solution was functionalized with oligonucleotide by first reacting one milliliter of the colloidal gold solution with 50 μL of a 100 μM solution of DSP in DMF for 15 minutes. A solvent exchange was performed by spinning down the modified colloidal gold samples for 40 min and suspending in 500 μL HEPES based buffer at pH 8.0. Coating of the gold nanoparticles with DSP was followed by the immobilization of 10 μL of 1000 μM dT₂₀ for three hours. Unreacted DSP sites on the colloidal gold were capped with 50 μL of 4 mM tris(hydroxymethyl)aminomethane (Tris). Hybridization was performed by the addition of 10 μL of 100 μM dA₂₀ and letting the solution react overnight. Samples were concentrated by centrifuging for 40 minutes and removing the supernatant. The resultant samples are designated as Au-DSP-dT₂₀ and Au-DSP-dT₂₀-dA₂₀ for immobilized (ss) DNA and duplex respectively. Samples were also prepared that did not include the addition of DSP coupling reagent. These have been designated as Au-dT₂₀ and Au-dT₂₀-dA₂₀ to represent adsorption of (ss) DNA and the duplex.

2.2.7 Microgravimetry by Quartz Crystal Microbalance

A Quartz Crystal Microbalance (QCM) tracks a change in oscillating frequency over time to quantify mass developing on one side of a double coated gold crystal. This technique has proven to be quite powerful in describing surface interactions.^{19, 20, 24, 26, 50} Experiments were conducted on a CH Instruments (Austin, TX), model 400A with AT-cut quartz crystals provided by the instrument manufacturer. A schematic of the instrument is portrayed in Figure 2-2.

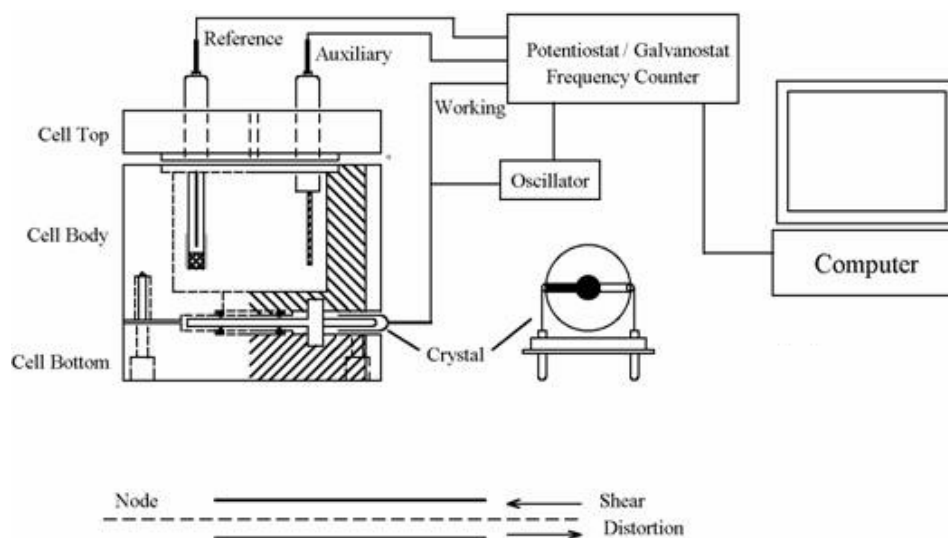


Figure 2-2. QCM Instrument. Schematic of the QCM instrument displaying crystal oscillation provided by CH Instruments.

Determining the mass gain on the surface as it relates to a change in frequency is achieved by the Sauerbrey equation.

$$\Delta f = -2f_o^2 \frac{\Delta m}{A\sqrt{\mu_q\rho_q}}$$

Excluding frequency (f) and mass (m), the parameters of the system are fixed [area (A), density (ρ_q), and shear modulus of quartz (μ_q)] which leads to a relation of 1 Hz equating to 1.34 ng of material adsorbed under experimental conditions. Frequency shifts (Δf) were determined to be the difference between two stable frequencies immediately following an injection of a sample and a minimum.

The gold surface of the quartz crystal was cleaned with 4:1 H_2SO_4 :30% H_2O_2 at $\sim 60^\circ\text{C}$ for 20 minutes just prior to running experiments. A baseline for the freshly cleaned gold surface was established in 150 μL of dimethyl formamide (DMF) to act as a reference before injecting 50 μL of 1 mM DSP in DMF. The sensor and cell were rinsed with a HEPES based buffer at pH 8.0 following the formation of a SAM of DSP.

Formation of either the DSP-matrix or DSP-dT₂₀ conjugate was done by placing 190 μ L of the same HEPES based buffer onto the surface before the addition of 10 μ L of 1 mM *n*-boc-1,4-phenylene diamine in DMF or 1 mM dT₂₀. Controls for each deposition step, consisting of solvent blanks, were performed in tandem with samples.

2.2.8 Electrochemistry

Cyclic voltammetry was used to evaluate the surface coverage on gold by means of two types of experiments. The redox behavior of a modified electrode in contact with supporting electrolyte was monitored in order to determine the surface coverage of redox active DSP. The redox couple of the electroactive species Fe^{III}(CN)₆³⁻ / Fe^{II}(CN)₆⁴⁻ was measured by monitoring the drop in peak current as a result of an increase in the diffusion layer thickness. The former experiment can yield the number of coulombs transferred and imply the number of moles on the surface, while the latter monitors the current as a function of sweep rate. The peak current (i_p) for a reversible system is defined by the Randles-Sevcik equation:

$$i_p = 2.69 \times 10^5 n^{3/2} A D^{1/2} C \nu^{1/2}$$

where n is the stoichiometric electron equivalence, A represents the area of the electrode, D is the diffusion coefficient, C is the concentration of the solution and ν is the scan rate.⁵¹ For a reversible reaction, as in the case for Fe^{III}(CN)₆³⁻ / Fe^{II}(CN)₆⁴⁻, we would expect the anodic peak current to be equal to the cathodic peak current. The CV experiment was performed by scanning negatively, from 0.4 V until Fe(III) is reduced to Fe(II) as determined by a peak for the cathodic current. The scan is reversed until Fe(II) is oxidized to Fe(III) generating a peak anodic current.

Measurements were made on a CH Instruments (Austin, TX), model 400A with a Ag/AgCl reference electrode and Pt auxiliary electrode provided by the instrument manufacturer. The parameters for cyclic voltammetry were as follows: 0.4 V as an initial voltage, 0.4 V as a high voltage, -0.3 V as a low voltage, negative scan polarity, a scan rate (ν) of 0.1 V/s, two sweep segments, and a sensitivity of 1×10^{-4} A/V.

The redox behavior of a SAM in contact with supporting electrolyte was performed utilizing the gold electrode of the QCM cell. Electrodes were reacted with 1 mM DSP in DMSO. The reaction proceeded for 30 minutes before washing with HEPES based buffer at pH 8.0 and reacted with 10 μ L of either 1 mM *n*-*boc*-1,4-phenylene diamine or 1000 μ M dT₂₀ solution overnight. The QCM cell was filled with a 100 mM solution of KCl at which point cyclic voltammetric measurements were performed.

To study the redox behavior of a modified electrode in contact with the electroactive $\text{Fe}^{\text{III}}(\text{CN})_6^{3-} / \text{Fe}^{\text{II}}(\text{CN})_6^{4-}$ redox couple, glass slides 1'' \times 0.25'' \times 0.04'' with a Ti/Au coating from EMF Corporation (Ithaca, NY) were used as a working electrode. A 1 mM solution of $\text{K}_4\text{Fe}(\text{CN})_6$ with 0.1 M KCl was prepared by weighing out 0.042 g of $\text{K}_4\text{Fe}(\text{CN})_6$ supplied by J.T. Baker (Phillipsburg, NJ), 0.745 g of KCl from EM Science (Lawrence, KS) and diluting to 100 mL with deionized water.

Slides were placed in a 1.5 mL cryogenic tube with 1.2 mL of 1 mM DSP in dimethyl sulfoxide (DMSO). Slides were allowed to react for 30 minutes before washing with HEPES based buffer at pH 8.0 and reacted with 1 mM of either *n*-*boc*-1,4-phenylene diamine or a dT₂₀ solution overnight. Slides were mounted to a clip and partially immersed in solution exposing 1.3 cm² to the solution, at which point cyclic voltammetric measurements were performed.

2.2.9 Surface Plasmon Resonance

Surface Plasmon Resonance (SPR) monitors a change in refractive index of a medium immediately above a gold surface. This is achieved by directing plane polarized monochromatic light onto a surface conducive to plasmon resonance and determining the angle of maximum absorbance by monitoring the reflected light. Surface plasmon excitation of gold involves the light-induced motion, around 520 nm, of all the valence electrons.^{50, 52} The exact wavelength and angle at which SPR occurs is dependant on the index of refraction on the gold surface.

The formation of a SAM on a gold surface can be monitored by observing a shift in the angle of absorbed, plane polarized, incident light ($\Delta\theta$) at which SPR occurs. The change in angle is related to the change in refractive index (Δn) and the geometrical thickness (d) by the following equation.²⁴

$$\Delta\theta = \Delta n d$$

Unfortunately, layers (d) less than 200 Å can not be determined from a single wavelength SPR measurement.^{53, 54} The Biacore X, which will be utilized for experiments, from Biacore (Sweden), translates $\Delta\theta$ and Δn into an increase in response units relating to a binding event on the surface.

Some debate has revolved around whether SPR can accurately describe the amount of single stranded DNA on a surface since it can take on two orientations, either lying down parallel to the surface or upright perpendicular to the surface.⁵⁵ The difference in dielectric constant (ϵ) between the two states is only 0.1 where the dielectric constant is related to the refractive index by $\epsilon = n^2$.⁵⁶ Considering that single stranded DNA is likely to take on an orientation that is a combination of the two states, parallel or

perpendicular to the surface, the experimental error from assuming either state would be minimal. Even if each strand took on a single orientation the greatest error would fall in the range of 12-15% of the deduced coverage.⁵⁵

Experiments were conducted to demonstrate (1) the binding of DSP to the gold sensor surface (2) immobilization of an amine terminated dT₂₀ along with matrix and (3) hybridization with dA₂₀. As done with electrochemical experiments, a gold sensor chip BR-1005-42 from Biacore was cleaned with 4:1 H₂SO₄:30% H₂O₂ at ~60°C for 20 min while being careful not to foul the sensor interface. Following the cleaning step, a SPR baseline of bare gold was collected as a reference. The sensor was removed from the instrument and exposed to a 1 mM solution of DSP in DMF for 20-30 minutes. Another SPR measurement was taken to determine a shift attributed to the formation of a SAM of DSP. Solutions of amine terminated dT₂₀ were allowed to react with the sensor surface for immobilization over flow channel two (Fc₂) at a flow rate of 10 µL/min. With the surface saturated with dT₂₀, solutions of *n*-boc-1,4-phenylene diamine in HEPES based buffer were flown over the sensor surface, again at 10 µL/min, in an effort to fill the unoccupied spaces between dT₂₀ strands. Following saturation of the surface with dT₂₀ and matrix, solutions of complimentary (dA₂₀) and non-complimentary oligonucleotide (ncDNA) were passed over both sensor surfaces (Fc₁ and Fc₂) to demonstrate hybridization at the same flow rate of 10 µL/ min.

With the polythymidilic acid (dT₂₀) probe immobilized to the surface a known concentration of polyadenylic acid (dA₂₀), typically ten times the concentration of dT₂₀ was added maintaining buffer conditions and allowed to hybridize with the immobilized dT₂₀.

2.2.10 MALDI-TOF Mass Spectrometry

A pulsed laser beam is applied to a crystalline sample, consisting of sample encased in matrix, that the matrix absorbs and transfers energy to the analyte which is subsequently desorbed and ionized. Since a pulsed laser source is used, a time of flight detector (TOF) can be utilized to separate ionized species based on their mass to charge ratio (m/z). Analysis by MALDI is governed by the efficiency of the matrix to transfer energy to the analyte in such a way as to induce desorption and ionization. For a more in-depth discussion on MALDI refer to section 1.2.1.

Three different MALDI-TOF experiments were designed to characterize the behavior of the SAM on gold, determine an optimal ratio of matrix:analyte, and investigate multi-component SAMs with colloidal gold.

The first experiment addressed attachment mechanisms on a gold MALDI target plate (Bruker Daltronics; Germany). The behavior of physisorbed samples was studied by placing 2 μL of 1000 μM dT₂₀ onto a gold MALDI plate and allowing adsorption to occur for one hour before adding 2 μL of 100 μM dA₂₀. Chemisorption was evaluated by attaching DSP then immobilizing an oligonucleotide labeled with a primary amine. The DSP linked oligonucleotide was prepared by adding 2 μL of 1 mM DSP in DMF onto the plate allowing attachment to occur for 30 minutes before washing and adding 2 μL of 1000 μM dT₂₀. The immobilization was allowed to proceed for one hour before adding 2 μL of 100 μM dA₂₀. Along with these samples a control well was prepared in the same manner as the DSP linked oligonucleotide but without the immobilized species. Table 2-1 outlines the content of each sample and gives each a generic name.

Table 2-1. MALDI Experiment 1. Matrix describing the compounds used to prepare each sample for an evaluation of the effects of mode of adsorption on the laser desorption ionization of oligonucleotides.

Sample	MALDI Plate				
	DSP	dT ₂₀	dA ₂₀	Matrix	Tris
A1					
B1		2 nmol			
C1		2 nmol	200 pmol		
D1	<input checked="" type="checkbox"/>	2 nmol			
E1	<input checked="" type="checkbox"/>	2 nmol	200 pmol		

A second experiment focused on the immobilization of a mixed SAM of matrix and oligonucleotide on a gold MALDI target plate over a range of concentrations. The DSP linked samples were prepared by adding 2 μ L of 1 mM DSP in DMF onto the plate and allowing attachment to occur for 30 minutes. Concentrations of oligonucleotide from 10 μ M-10 nM of dT₂₀ in tenfold increments, with 2 μ L spotting, were immobilized to the gold MALDI target plate by means of DSP. Following immobilization of dT₂₀ by DSP, the unreacted sites of DSP were bound to matrix with 2 μ L spotting of 1 mM *n*-boc-1,4-phenylene diamine. Hybridization with dA₂₀ was performed by adding ten times the amount of dT₂₀ applied to the plate. A detailed outline describing each of the samples and controls is given in Table 2-2.

Table 2-2. MALDI Experiment 2. Matrix describing the compounds used to prepare each sample for an evaluation of the effects of matrix and oligonucleotide concentration on the laser desorption ionization MS of oligonucleotides (* - adsorbed duplex).

Sample	MALDI Plate				
	DSP	dT ₂₀	dA ₂₀	Matrix	Tris
A2					
B2	<input checked="" type="checkbox"/>			<input checked="" type="checkbox"/>	
C2		20 pmol*	200 pmol*	<input checked="" type="checkbox"/>	
D2	<input checked="" type="checkbox"/>	20 pmol	200 pmol	<input checked="" type="checkbox"/>	
E2	<input checked="" type="checkbox"/>	2 pmol	20 pmol	<input checked="" type="checkbox"/>	
F2	<input checked="" type="checkbox"/>	200 fmol	2 pmol	<input checked="" type="checkbox"/>	
G2	<input checked="" type="checkbox"/>	20 fmol	200 fmol	<input checked="" type="checkbox"/>	

The final experiment involved the use of colloidal gold. For each sample in these experiments oligonucleotide was immobilized both to the gold plate and gold colloid. As done before, 2 μL of 1 mM DSP in DMF was spotted onto the MALDI plate and set aside for 30 minutes. Applying DSP to colloidal gold consisted of reacting one milliliter of the colloidal gold solution with 50 μL of a 100 μM solution of DSP for 15 minutes (as done with gel electrophoresis). The addition of 4 mM Tris followed the reaction with immobilizing species (as done with gel electrophoresis). Table 2-3 outlines the samples processed for this round of experiments.

Table 2-3. MALDI Experiment 3. Matrix describing the compounds used to prepare each sample for an evaluation of the effects of laser desorption ionization of oligonucleotides on colloidal gold.

Sample	MALDI Plate					Colloidal Gold	
	DSP	dT ₂₀	dA ₂₀	Matrix	Tris	DSP	Matrix
A3	<input checked="" type="checkbox"/>	<input checked="" type="checkbox"/>	<input checked="" type="checkbox"/>				
B3	<input checked="" type="checkbox"/>	<input checked="" type="checkbox"/>	<input checked="" type="checkbox"/>			<input checked="" type="checkbox"/>	<input checked="" type="checkbox"/>
C3	<input checked="" type="checkbox"/>	<input checked="" type="checkbox"/>	<input checked="" type="checkbox"/>		<input checked="" type="checkbox"/>		
D3	<input checked="" type="checkbox"/>	<input checked="" type="checkbox"/>	<input checked="" type="checkbox"/>		<input checked="" type="checkbox"/>	<input checked="" type="checkbox"/>	
E3	<input checked="" type="checkbox"/>	<input checked="" type="checkbox"/>	<input checked="" type="checkbox"/>		<input checked="" type="checkbox"/>	<input checked="" type="checkbox"/>	<input checked="" type="checkbox"/>
F3	<input checked="" type="checkbox"/>	<input checked="" type="checkbox"/>	<input checked="" type="checkbox"/>	<input checked="" type="checkbox"/>			
G3	<input checked="" type="checkbox"/>	<input checked="" type="checkbox"/>	<input checked="" type="checkbox"/>	<input checked="" type="checkbox"/>		<input checked="" type="checkbox"/>	
H3	<input checked="" type="checkbox"/>	<input checked="" type="checkbox"/>	<input checked="" type="checkbox"/>	<input checked="" type="checkbox"/>		<input checked="" type="checkbox"/>	<input checked="" type="checkbox"/>
I3		<input checked="" type="checkbox"/>	<input checked="" type="checkbox"/>				
J3		<input checked="" type="checkbox"/>	<input checked="" type="checkbox"/>			<input checked="" type="checkbox"/>	<input checked="" type="checkbox"/>

The three outlined MALDI experiments were conducted on a Bruker Daltronics, Autoflex TOF/TOF. The gold target plate was also supplied by Bruker Daltonics (Germany) and cleaned with 4:1 H_2SO_4 :30% H_2O_2 before depositing samples.

CHAPTER 3.0

RESULTS

3.1.0 Analytical Methods

3.1.1 Molecular Modeling

The creation of a SAM of DSP on a gold surface through simulations of chemisorption and van der Waals interactions between DSP was performed. Minimization of the energy and dynamics simulations led to orientating the DSP fragment with the succinimidyl endgroup somewhat parallel to the gold surface and in what has been labeled a “lying-down” structure or striped phase.¹⁶ A second DSP fragment was brought into proximity of the first, immobilized fragment such that the succinimidyl endgroups of the two molecules were farthest apart and the thiol groups were the closest atoms between the two molecules. This orientation was chosen to mimic the steps of chemisorption of an intact DSP molecule leading to cleavage of the disulfide bond and deposition of one half of the identical DSP fragments. Chemisorption and van der Waals forces between the gold surface and DSP fragments on a sparsely populated surface generated a lying down configuration as seen in Figure 3-1.

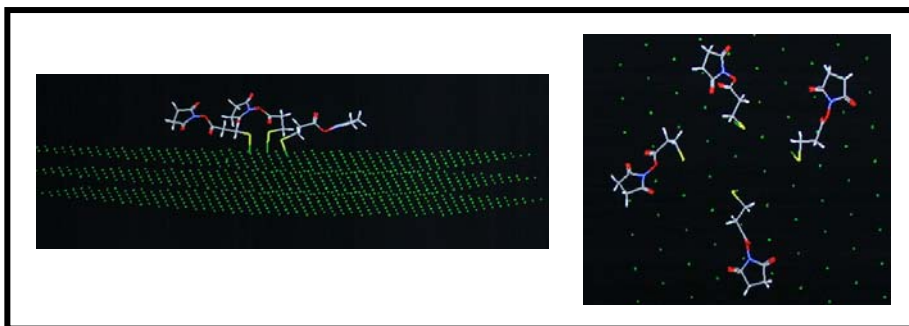


Figure 3-1. Lying Down Phase of SAM. Van der Waals interactions between molecules on a sparsely populated Au (1,1,1) surface.

Through examination of components of a stylized DSP monolayer, a favorable unit cell was determined as shown in Figure 3-2 to be $(\sqrt{3} \times \sqrt{3})d_{\text{Au}}$. The ordered array generates a total energy of 5291 kcal/mol in comparison to a random arrangement which gives 5898 kcal/mol of kinetic and potential energy as determined by dynamics simulations. The sulfur atoms, and subsequently the DSP fragment, are arranged atop the fcc lattice of a 2×2 cell of gold which agrees with the findings of Schreiber.¹⁶ In the same article, Schreiber makes the argument that sulfur adopts a tetrahedral (sp^3) configuration and interacts with three gold atoms in addition to the alkyl chain since it falls in the fcc hole on the gold surface. The sp^3 angle and steric forces arrange the alkyl segment of the DSP fragment such that the hydrogens on the alpha carbon to sulfur interact with the gold surface. Another force driving this conformation is the electronegative charge on the carbonyl being drawn to the positively charged gold atoms. The succinimidyl end group takes on a canted orientation, most likely, due to hydrophobic interactions between DSP fragments and charge interactions with the surface.

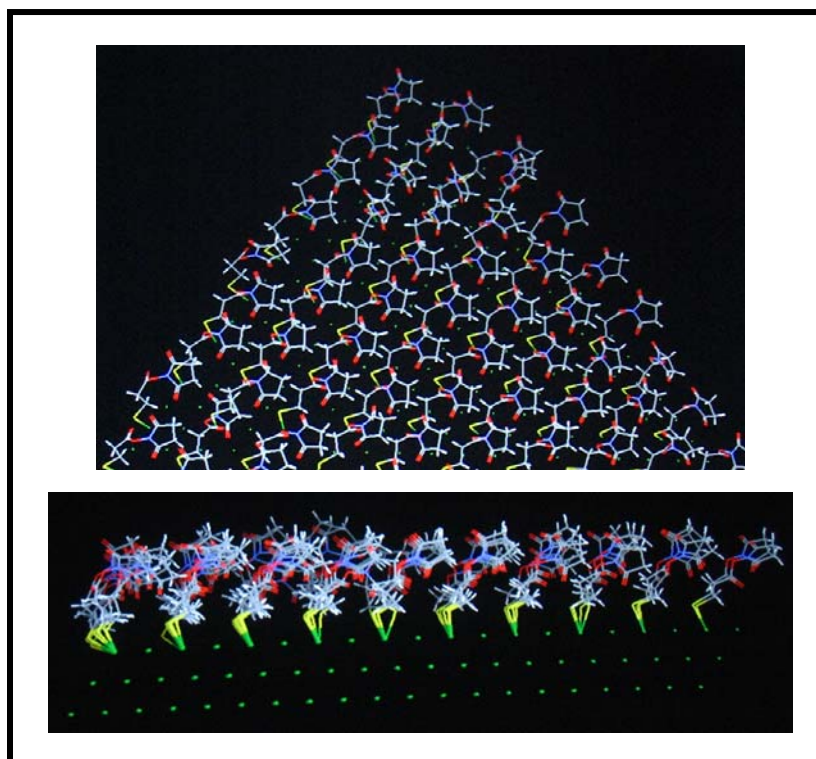


Figure 3-2. Upright Phase of SAM. The most energetically favorable configuration, as viewed normal and parallel to the surface, of a monolayer of DSP on Au (1,1,1) as determined through molecular modeling.

Even with a casual observation of the SAM, it is apparent that DSP fragments that lie on or near the edge of the gold (1,1,1) surface don't take on an orientation of the bulk. As a result, the outer two rows of the DSP lattice were not utilized in measurements outlined below.

The angle adopted by the DSP fragment in respect to the surface was estimated to be $57.1 \pm 1.6^\circ$ as shown in Figure 3-3. Schreiber suggests an angle of 70° for linear alkyls attached to a gold surface through a terminal sulfhydryl group.¹⁶ Differences in the attachment angle between DSP and the linear alkyl could be attributed to columbic interactions inherent to DSP that are absent in a non-polar alkane.

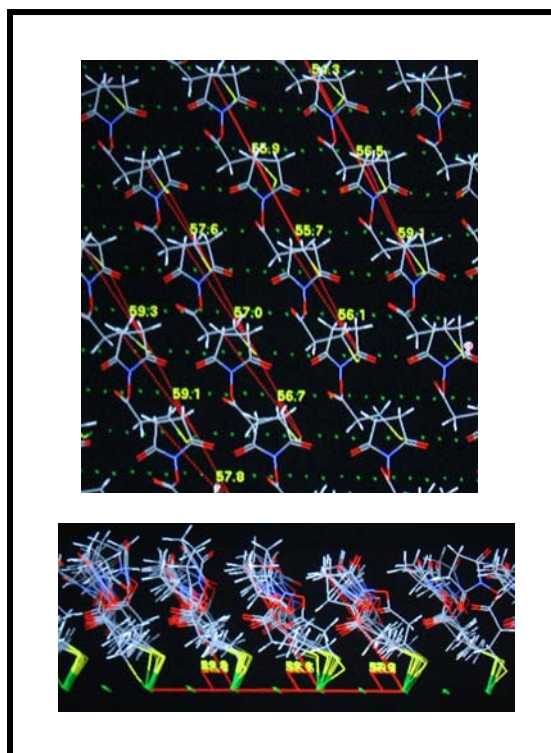


Figure 3-3. Surface Angle of DSP. Estimation of an attachment angle of DSP fragment with respect to the gold surface.

Another measurable aspect of the SAM is the height of the DSP fragment normal to the surface. As with the angle measurements, only molecules representative of the bulk were used to realize a height normal to the surface of 7.6 ± 0.2 Å as demonstrated in Figure 3-4. The height of the monolayer can also be derived mathematically from the trigometric relations:

$$\cos \theta = \frac{x}{d} \quad \text{and} \quad \sin \theta = \frac{y}{d}$$

Setting the length of the DSP fragment (d) to 9.2 Å and the angle (θ) to 57.1 yields $x = 5.1$ Å and $y = 7.7$ Å which is in agreement with the measured value.

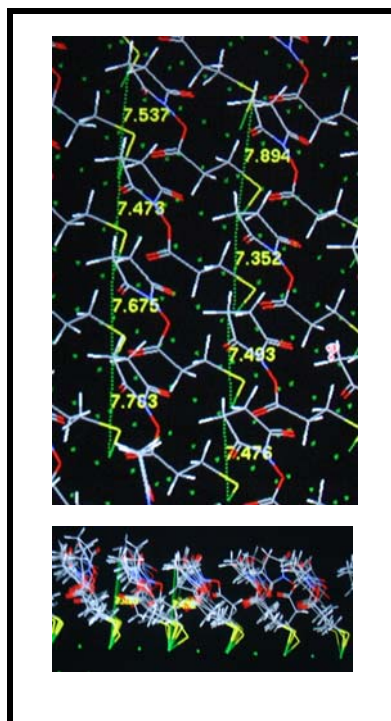


Figure 3-4. Height of DSP Monolayer. Estimation of the height of a DSP fragment roughly normal to the gold surface.

Knowing that the DSP fragments take on a $(\sqrt{3} \times \sqrt{3})d_{Au}$ hexagonal structure as described in the literature and as demonstrated here through molecular modeling, it is possible to determine a surface coverage of DSP on an atomically flat Au (1,1,1) surface.¹⁶ Since gold has an atomic diameter of 2.88 Å, it is possible to represent surface coverage of DSP in terms of picomoles per square millimeter by the following relation:

$$\frac{1 \text{ molecule}}{(\sqrt{3} \cdot 2.88) \cdot (\sqrt{3} \cdot 2.88) \text{ Å}^2} \left(\frac{1 \text{ mol}}{6.022 \times 10^{23} \text{ molecules}} \right) \left(\frac{1 \text{ Å}}{1 \times 10^{-7} \text{ mm}} \right)^2 \left(\frac{1 \times 10^{12} \text{ pmol}}{1 \text{ mol}} \right) = 6.67 \frac{\text{pmol}}{\text{mm}^2}$$

The software is also capable of determining close contact distances which proves to be a valuable tool in identifying inconsistencies in the SAM. Setting the maximum reportable close contact distance to 3.00 Å generates the measurements of Figure 3-5.

From the photograph it's clear that the majority of close contact distances hover around 2.4 Å with deviations coming, predictably, from the outer two rows.

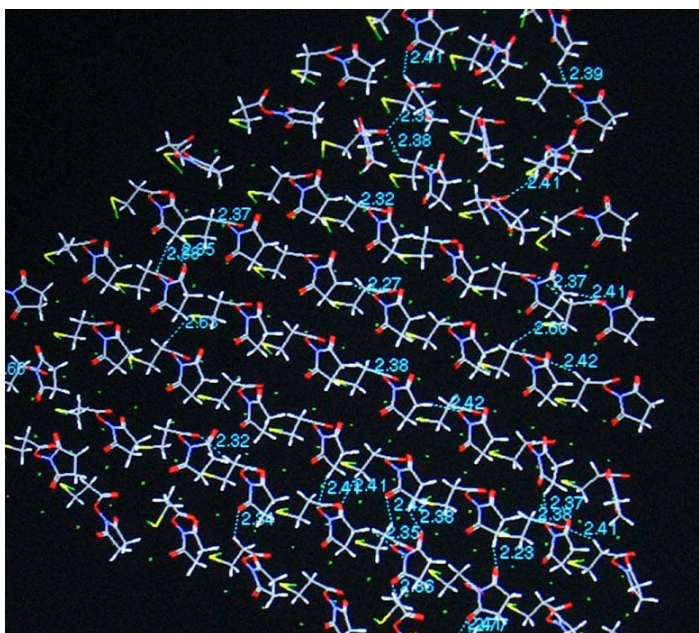


Figure 3-5. Spacing of DSP Monolayer. Display of close contact measurements demonstrating deviations in the SAM from the outer two rows.

The attachment of (ss) DNA to the DSP monolayer through a terminal amine linked by a six carbon spacer arm was a final model under evaluation. The dT₂₀ oligomer chosen for modeling was also utilized experimentally to allow comparison of results. From Agbasi-Porter and Tinland we can estimate an approximate value for the radius of gyration of a single strand oligomer attached terminally to a surface by the following equation:

$$d = L\sqrt{N}$$

The distance between bonds is represented by L , where L is approximately 1.55 Å.^{23, 57}

In determining N , the number of bonds for (ss) DNA, one must recognize that there are six single bonds in the backbone of each nucleotide (C5'-O-P-OC3'-C4'-C5') in addition to a six carbon spacer arm at the end. For the dT₂₀ $N = 20 \times 6 + 6 = 126$ bonds.

Substituting N and L into the equation yields $d = 1.7$ nm. The area swept by the tethered oligomer can be determined by:

$$area = \pi d^2 \cos^2 \theta$$

This equation demonstrates that as the radius of the tethered (ss) DNA becomes longer (increasing d), the surface area swept increases with minor changes in attachment angle (θ). An accurate value for the angle between the SAM and the oligomer was attempted through molecular modeling but a clear representation of the optimal angle proved elusive. At 60° the potential energy of the system was approximately 2526 ± 166 kcal/mol. With the oligomer in a lying down configuration, the potential energy was estimated at 2394 ± 159 kcal/mol. Given that intermediate angles between 60° and 0° fall in the range of 2300-2700 kcal/mol a favorable configuration that falls clearly beyond the standard deviation could not be accurately determined. As the surface becomes more populated with oligomer strands van der Waals forces between immobilized (ss) DNA could influence a more upright position.

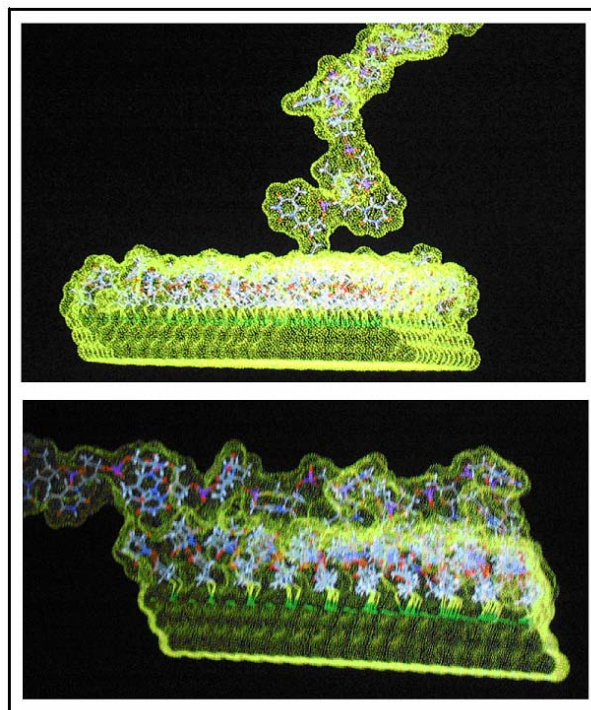


Figure 3-6. Orientation of Immobilized Oligomer. Connolly surface representation of a terminally attached (ss) DNA fragment at 60° with respect to the SAM and in intimate contact with the SAM.

Focusing on an optimal density of (ss) DNA for hybridization rather than an attachment angle of (ss) DNA could prove to be more useful information than trying to determine an attachment angle. Castelino and Peterlinz claim optimal hybridization for a 20mer occurring at densities of 0.04 molecules/nm² and 0.052 molecules/nm² respectively.^{53, 58} Applying 0.052 molecules/nm² (19.2 nm²/molecule) to the area occupied by a tethered nucleotide outlined above yields an unsolvable relation for an attachment angle.

$$\cos^2 \theta = \frac{\text{area}}{\pi \cdot d^2} = \frac{19.2 \text{ nm}^2}{\pi \cdot (1.7 \text{ nm})^2} = 2.1$$

The impossibility arises because the value for the swept area is far greater than any area the radius of gyration could sweep out. The apparently low surface density necessary for

efficient hybridization can be explained by the conformation of the duplex. With hybridization, the oligomer transforms from a random coil, characteristic of Gaussian chain behavior, to a nearly fully extended duplex (approximately $0.34 \text{ nm/bp} \times 21 \text{ bp} = 7.1 \text{ nm}$) which gives a solvable relation.

$$\cos^2 \theta = \frac{\text{area}}{\pi \cdot d^2} = \frac{19.2 \text{ nm}^2}{\pi \cdot (7.1 \text{ nm})^2} = 0.12$$

$$\theta = 70$$

Surprisingly, an angle of 70° for the duplex is the same angle adopted by the tethered alkyl chains cited by Schreiber.¹⁶

Measurements based on molecular modeling for the SAM of DSP and the attachment of oligomer will be compared to analytical results throughout Section 3.2.

3.1.2 Atomic Force Microscopy

All of the samples prepared for AFM demonstrated a prominent blue shift in wavelength indicating that significant aggregation of the sample was occurring.^{1, 46} Preparation of the samples as done in section 2.2.5, which minimized aggregation in solution, could have lead to different AFM results for some of the samples. The unmodified colloidal gold sample demonstrated the highest degree of aggregation yielding the tallest and widest profiles amongst all the samples (Figure 3-7) on the order of microns in size. This close contact arrangement of gold nanoparticles is in agreement with literature findings.^{46, 50, 59} Cumberland and Strouse suggest that the tannic acid used to stabilize the surface of the colloidal particles in solution encourages agglomeration upon drying.⁶⁰

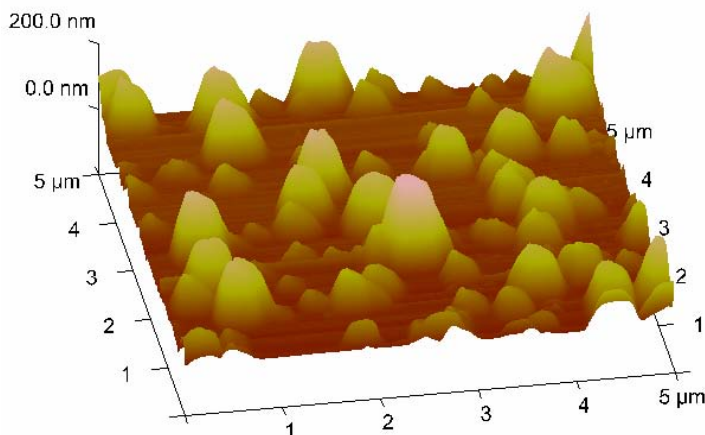


Figure 3-7. AFM Measurement of Au. AFM results of unmodified gold nanoparticles.

Colloidal gold with DSP deposited on the surface demonstrated aggregation but not to the same extent as seen in the colloidal gold sample. The size and shape of the aggregates were noticeably smaller and there was a degree of uniformity that was not seen in the colloidal gold sample (Figure 3-8). If hydrolysis of the DSP layer had occurred, this would generate an electrical double layer resulting in a net negative surface charge repelling similar nanoparticles.^{1, 25} Also found on the Au-DSP sample substrate were what appeared to be crystals. Whether the crystals, not found in the other samples under evaluation, were silicon fragments resulting from breaking a wafer into 1"×1" pieces or a large mass of DSP functionalized colloidal gold is unclear.

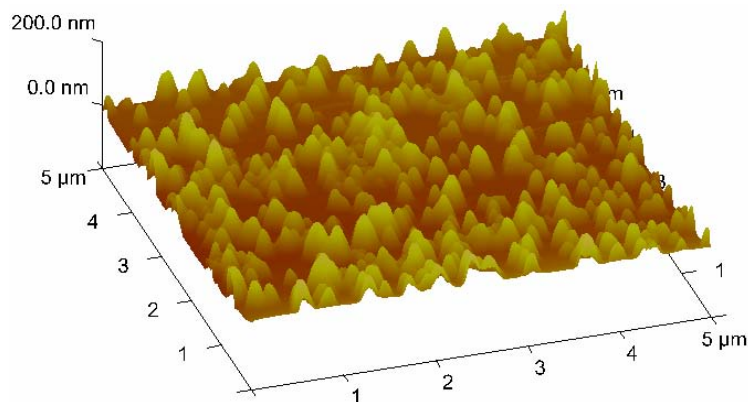


Figure 3-8. AFM Measurement of Au-DSP. DSP functionalized gold nanoparticles.

The colloidal gold sample with *n*-boc-1,4-phenylene diamine linked to the surface through DSP demonstrated a marked difference in aggregation from the other samples under evaluation. The aggregates formed a series of dendrimer like clusters (Figure 3-9). The dendrimer-like clusters were consistent throughout the 60 $\mu\text{m} \times 60 \mu\text{m}$ scan and displayed an even spacing. Joshi and Shirude described amino acid labeled colloidal gold particles as “open, string-like structures” held together by interparticle hydrogen bonding.⁵⁹ If *n*-boc-1,4-phenylene diamine was attached to the surface by an amide bond with DSP as intended, it could participate in pi-pi interactions in addition to hydrogen bonding.

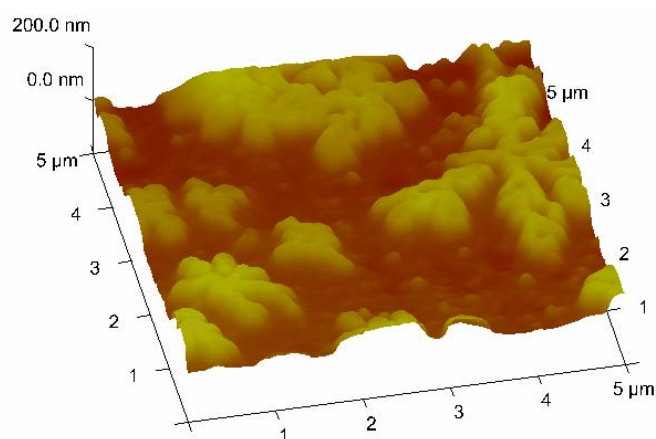


Figure 3-9. AFM Measurement of Au-DSP-Matrix. Gold colloid labeled with DSP linked to *n*-boc-1,4-phenylene diamine.

A fourth sample analyzed was the terminal amine labeled dT₂₀ oligonucleotide deposited on the gold surface through DSP. The clusters formed in this sample were analogous to what was seen in the DSP labeled colloidal gold. A distinguishing feature of this sample from the Au-DSP sample is larger aggregates with a rounder profile (Figure 3-10).

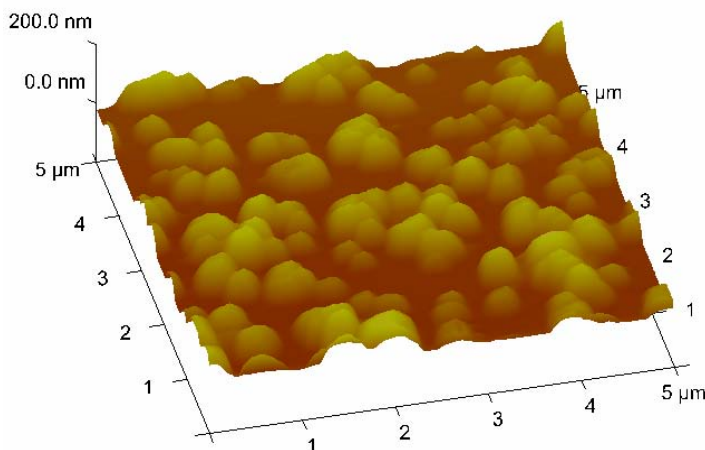


Figure 3-10. AFM Measurement of Au-DSP-dT₂₀. Gold colloid with DSP linked to primary amine labeled oligomer (dT₂₀).

3.1.3 Infrared Spectroscopy

Evaluating the reaction between DSP and a primary amine by infrared would involve comparing IR spectra for DSP, the primary amine and the DSP-amine conjugated species. Bands characteristic to DSP, but not the crosslinked species, include the bands associated with the ester at 1817 cm^{-1} , 1788 cm^{-1} and 1751 cm^{-1} .²² These bands represent the stretch of the ester, and the in-phase and out-of-phase carbonyl stretches of the succinimidyl endgroup (NHS) respectively.⁶¹ Other characteristic bands are derived from bonds with nitrogen: C-N stretch at 1218 cm^{-1} and C-N-O stretch at 1077 cm^{-1} .²² The red trace of Figure 3-11 displays experimental results for the FT IR measurement of DSP. Bands associated with C-H stretch, bend and rocking have been removed due to interference arising from the polyethylene substrate.

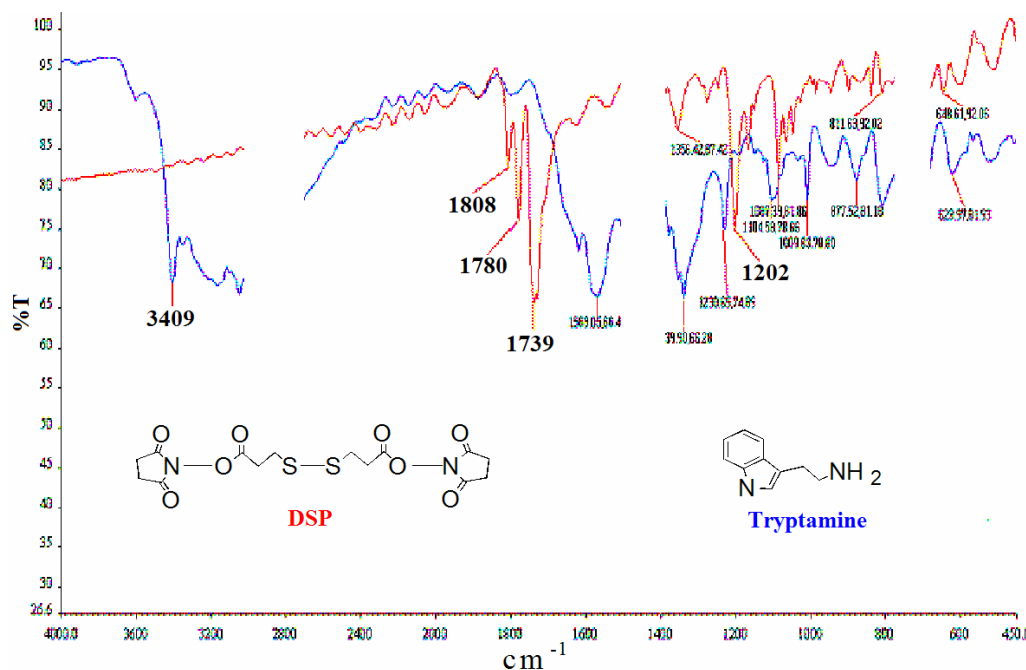


Figure 3-11. IR Spectra of DSP and Tryptamine. Overlay of FTIR data from DSP(red) and tryptamine(blue) with C-H bands removed.

There is a slight shift in the location of the bands for DSP but their relative intensities and shape are consistent with literature findings.²² Characteristic bands for tryptamine include two weak bands for asymmetrical and symmetrical N-H stretching near 3500 cm^{-1} and 3400 cm^{-1} for the primary amine.⁵ The broad band for the indole secondary amine, in the range of $3350\text{--}3310\text{ cm}^{-1}$, shoulders one of the primary amine bands.

The distinctive bands of NHS that identified DSP will be absent with the formation of the conjugate. Characteristic bands displayed by the conjugate would include a single band in the vicinity of 3350 cm^{-1} attributed to N-H stretching of a secondary amide in the solid state.^{5, 62} Secondary acyclic amides in the solid state display an amide I band around 1640 cm^{-1} and an amide II band in the region $1570\text{--}1515\text{ cm}^{-1}$

as suggested by Silverstein et al.⁵ Results of FT IR analysis by means of attenuated total reflection (ATR) are displayed in Figure 3-12.

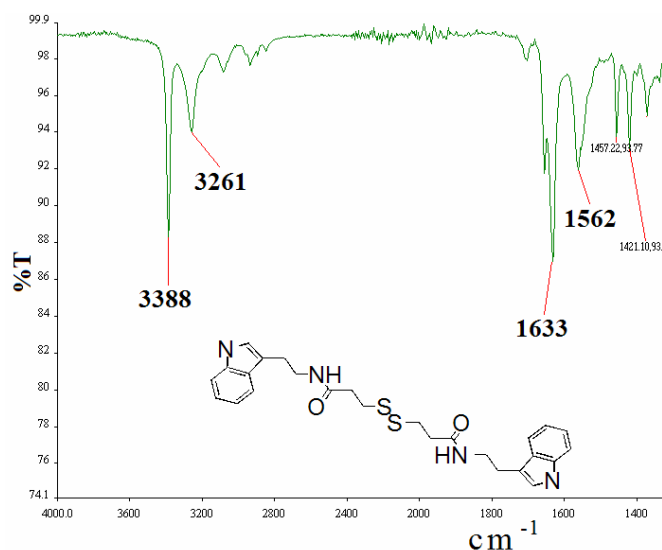


Figure 3-12. IR Spectra of Conjugate. FT IR-ATR data for the conjugate of DSP and tryptamine.

The absence of the NHS bands along with the presence of the amide I and II bands are evidence of the formation of the conjugate between DSP and tryptamine. The band at 3261 cm^{-1} is most likely the N-H stretching band of the indole ring that appeared as a broad band in the FT IR analysis of tryptamine.

3.1.4 ^1H Nuclear Magnetic Resonance

In addition to infrared data, ^1H NMR is quite effective at demonstrating the amide formation of DSP with an amine. Unfortunately, the collection of ^1H NMR spectra involved compromises that influenced the quality of the data. One such concession made was the use of 5 mL of colloidal gold that results in less than 0.1 mg of immobilized sample for analysis; whereas, a typical analysis requires about 10 mg of sample per 0.5 mL of solvent. Clean up of the sample was minimal, in an effort to minimize sample loss, which resulted in contamination of the sample with water ($\delta 1.55$).⁵ Regardless,



With the formation of a SAM of conjugate (DSP- *n*-*boc*-1,4-phenylene diamine) on colloidal gold, peak shapes are broadened, indicating restricted movement, and multiplicity can no longer be determined.^{15, 63} This makes determining connectivity difficult, but an interpretation of the spectra is possible with peak area and chemical shift tables since the structure is known. Chemical-shift-equivalent benzylic protons on *p*-monosubstituted benzene rings appear at δ 7.175 which could be interpreted as the peak seen at δ 7.2 in Figure 3-13.⁵ Applying Shoolery's rule (the sum of the substituent constants for the attached functional groups is added to 0.23 to determine a shift) to the α and β methylenes of the thiol gives:

$$\delta_{\alpha} = 0.23 + \sigma_{SH} + \sigma_{CH_2} = 0.23 + 1.64 + 1.32 = 3.19$$

$$\delta_{\beta} = 0.23 + \sigma_{CO} + \sigma_{CH_2} = 0.23 + 1.50 + 1.32 = 3.05$$

The calculated shift is close to the observed peaks at δ 2.9 and δ 2.8 both yielding a peak area of 2.0.⁵ As eluded to earlier, attempts to produce a dry sample were not taken in the interest of conserving the limited amount of sample which resulted in a large peak at δ 1.55 associated with water in a D₂O solvent.^{5, 15} The next peak under scrutiny is δ 1.25 with a peak area of 3.1 and relatively broad in shape. A broad peak is characteristic of hydrogen bonding with slow to intermediate exchanges.⁵ Hasan et al. associate the peak of δ 1.0 with a proton bound to the thiol or adsorbed to the gold surface.¹⁵ This would mean that the two protons associated with the secondary amines overlap with the benzylic protons at δ 7.2. This leaves a final peak, and the last chemical-shift-equivalent protons, at δ 0.8 of reduced area 8.7 to be the protons on the *t*-boc group.

If deposited DSP had not reacted with *n*-boc-1,4-phenylene diamine then there would be a single peak, of area 4, around δ 2.7 correlating to the protons on the succinimidyl ester (NHS). Hasan et al. made the distinction between immobilized thiol compounds and those free in solution by the absence or presence of exchanges.⁶³ If the conjugate were free in solution there should be narrower peaks with triplets for the α and β methylenes of the thiol.

3.1.5 UV-Vis Absorbance

Through UV-Vis measurements of colloidal gold it was possible to determine an optimal ratio of DSP:colloidal gold to allow maximum coverage of the gold surface while minimizing aggregation. The gold nanoparticles are prepared with an electrical double layer of citrate resulting in a negative charge on the surface.⁶⁹ With the addition of salts or excess label to solution the negative charge can be partially masked and allow nanoparticles to come within range of van der Waals attraction.¹ In this region the

particles begin to coalesce, which reduces surface area and results in a precipitate, concurrent with an observable shift in color from red to blue. By monitoring the absorbance of the solution at 580 nm it is possible to determine the aggregation point of the gold nanoparticle.

To 100 μL aliquots of colloidal gold, various amounts of DSP ranging from 0.01 nmol to 100 nmol in ten fold increments were added to determine an aggregation point by UV-Vis absorbance measurements. As Figure 3-14 demonstrates, the zeta potential occurs around 1 nmol of DSP for 100 μL of colloidal gold. Subsequent experiments over a narrower range of DSP concentrations demonstrated that an ideal working ratio appeared to be 0.5 nmol for every 100 μL of colloidal gold. At a loading concentration of 5 nmol DSP per milliliter of colloidal gold the absorbance band reflects a similar shape to that of the unmodified colloidal gold suspension.

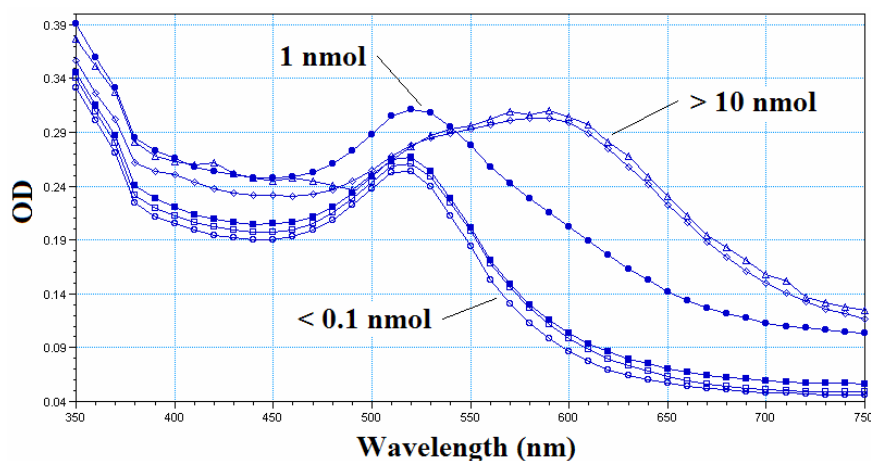


Figure 3-14. UV-Vis Absorbance Spectra of Au-DSP. Overlay of UV-Vis data outlining increasing nature of colloid aggregation, associated with a blue shift in peak wavelength, with increasing concentration of DSP for 100 μL aliquots of colloidal gold.

Since the available surface area of the gold nanoparticle has been defined, section 2.1.1, it is possible to estimate the surface coverage for DSP at the zeta potential.

Utilizing the surface area of colloidal gold per volume of solution and applying the optimal concentration values for DSP determined in this section gives:

$$(0.1\text{mL})\left(\frac{1.8 \times 10^3 \text{ mm}^2}{\text{mL}}\right) = 1.8 \times 10^2 \text{ mm}^2 \text{ of surface area}$$

$$\frac{500 \text{ pmol}}{1.8 \times 10^2 \text{ mm}^2} = 2.8 \text{ pmol} / \text{mm}^2$$

Comparing this concentration for DSP on colloidal gold to the amount of DSP bound on an atomically flat Au (1,1,1) surface (6.67 pmol/ mm²) is tempting but some considerations need to be addressed before making a comparison. The shape of the colloidal gold particle was assumed to be spherical to ease in calculating the surface area where in actuality the nanoparticle is truncated octahedron in shape which consists of many facets of unknown proportions.^{17, 23, 64} Another consideration is that the multiple facets offer several lattice planes all of which are of differing packing density than Au (1,1,1).^{64, 65} It's possible that the zeta potential and saturation point don't coincide, considering citrate and DSP exhibit different charges, which would result in a loading density for DSP less than saturation. Regardless, the saturation density for DSP on colloidal gold is within the same order of magnitude as that on an Au (1,1,1) surface.

Cumberland and Strouse suggest that the tendency of particles to coalesce can be overcome by increasing the Lewis basicity of surface groups.⁶⁰ This idea was tested by capping unreacted sites of DSP, following an incubation step with dT₂₀, with Tris. In a basic solution, the hydroxy groups on bound Tris act as proton acceptors giving them a net positive charge. Five vials with colloidal gold were prepared such that one was a control, two were functionalized with DSP for the immobilization of dT₂₀ (Au-DSP-dT₂₀), and the final two were allowed to adsorb dT₂₀ (Au dT₂₀). These vials, as described

from left to right, are pictured in Figure 3-15 (frame A). Vials with immobilized dT₂₀ displayed a prominent blue color while the gold control demonstrated little change.

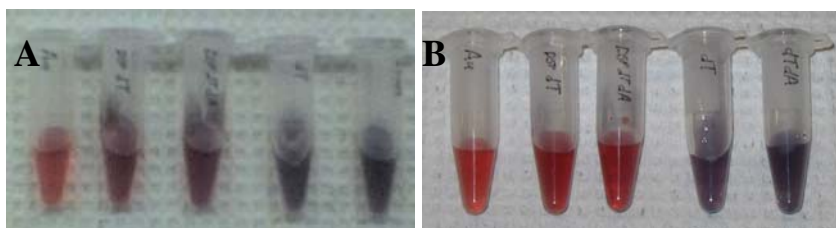


Figure 3-15. Phase Transition of Functionalized Colloidal Gold. Photographs displaying transition of DSP-dT₂₀ labeled colloidal gold from an aggregate (blue) in frame A to fine suspension (red) in frame B with the addition of Tris.

With the addition of Tris to all the vials, the DSP- dT₂₀ functionalized gold nanoparticles (second and third from the left in both frames A and B) exhibited a gradual color shift from blue back to red as demonstrated in frame B of Figure 3-15. Tris failed to modify the aggregated nanoparticles with dT₂₀ adsorbed to the surface (fourth and fifth vials from the left in both frames A and B) suggesting that Tris binds to the colloidal gold through DSP and not through a direct interaction with the surface. As Cumberland and Strouse suggested, it is possible to break apart an aggregate with the addition of a Lewis base to the surface.

An absorbance scan in the UV-Vis of the samples from Figure 3-15 following the addition of Tris is depicted in Figure 3-16. The adsorbed dT₂₀ exhibits a broad band attributed to aggregation while dT₂₀ immobilized through DSP displays the absorbance maximum associated with particles in a fine suspension.

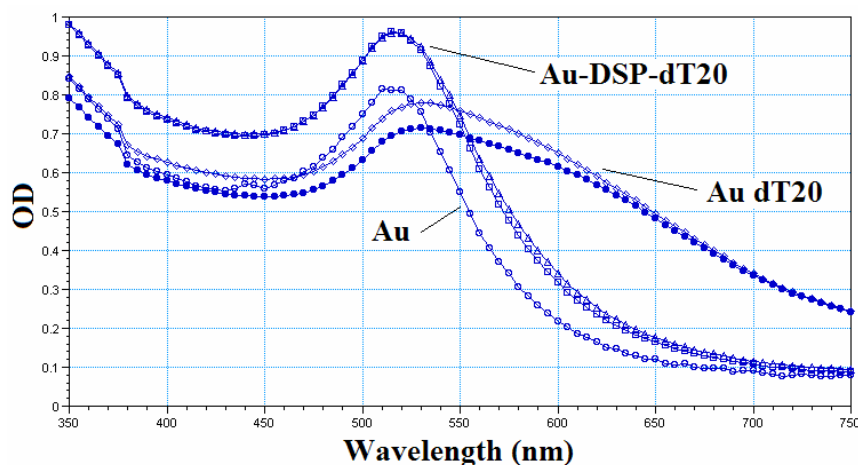


Figure 3-16. UV-Vis Absorbance Spectra of Colloidal Gold Samples. Overlay of UV-Vis data from vials in Figure 3-15 demonstrating aggregate nature of adsorbed oligomer (Au dT₂₀) in comparison to particulate nature of DSP linked oligomer (Au-DSP-dT₂₀).

3.1.6 Gel Electrophoresis

Oligonucleotide labeled colloidal gold samples were prepared for gel electrophoresis by physical adsorption and immobilized through DSP. Section 3.1.5 demonstrated how oligomers can attach to gold by means of physical adsorption or immobilization through a DSP linker. Following immobilization of oligonucleotide, unoccupied sites of unreacted DSP were capped with tris(hydroxymethyl)aminomethane (Tris). Since the gold nanoparticles absorb strongly at 520 nm they exhibit a red color that is visible as it passes through the gel. The bright red color of the colloidal gold samples allowed the migration progress of each sample to be monitored without the aid of a marker. This is critical because Sandström et al. noted that fluorescein labeled oligomers were quenched by gold nanoparticles.¹⁷ Experiments with UV-Vis in section 3.1.5 confirm the absorption band of colloidal gold encompasses the excitation and emission ranges of ethidium bromide (350-450 nm).

A control sample of gold colloid functionalized with DSP and capped with Tris was run in lane two of Figure 3-17 and appeared to run through the gel at approximately

the same rate as the oligonucleotide adsorbed on gold samples Au-dT₂₀ and Au-dT₂₀-dA₂₀ in lanes three and four respectively. The adsorbed duplex, Au-dT₂₀-dA₂₀, of lane 4 displays a blue tint suggesting aggregation. The Au-DSP-dT₂₀ and Au-DSP-dT₂₀-dA₂₀ samples in lanes 5 and 6 respectively display the fastest migration with the duplex trailing the single strand slightly.

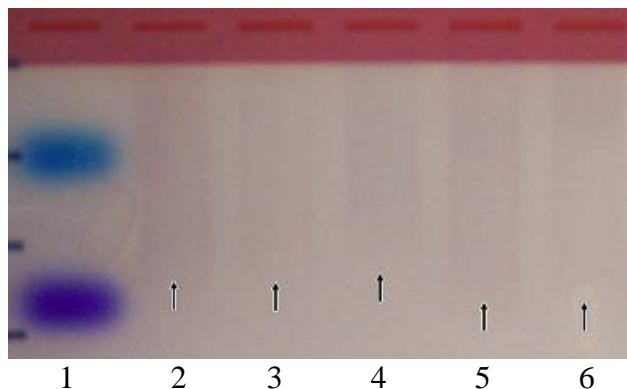


Figure 3-17. Gel Electrophoresis of Low Concentration Colloidal Gold Samples. Photograph of 1% agarose gel demonstrating tris capped gold nanoparticles in lane 2, Au-dT₂₀ and Au-dT₂₀-dA₂₀ (lanes 3,4) and Au-DSP-dT₂₀ and Au-DSP-dT₂₀-dA₂₀ (lanes 5,6) where the migrating front is suggested by arrows.

Observing the fluorescence of the gel (Figure 3-18) gives insight as to the mobility of duplex attached to the colloidal gold samples. Samples of single stranded oligomer (lanes 3, 5 and 7) failed to stain adequately with the intercalating agent ethidium bromide. The molecular weight standards from lane 1 were not used as an absolute determination of the weight of the colloidal gold samples but merely an indication of mobility since they are not a true representation of size, charge and shape of the colloidal gold samples. A calibration plot of the 50 base pair, molecular weight standards in lane 1 ($R^2 = 0.993$) yielded mobilities for Au-dT₂₀-dA₂₀ and Au-DSP-dT₂₀-dA₂₀ equivalent to that of 31 and 29 base pair oligonucleotides.⁶⁶ The intensities of the bands in lanes 4 and 6 are far lower than the reference duplex, dT₂₀-dA₂₀, of lane 8 suggesting that the majority of oligonucleotide is bound to the gold nanoparticle and

quenched. The saturation point for duplex on a gold nanoparticle was determined to be approximately 100 double strands /particle by Sandström et al. which is an order of magnitude less than what was attempted to load on these samples (4700 double strands /particle).¹⁷

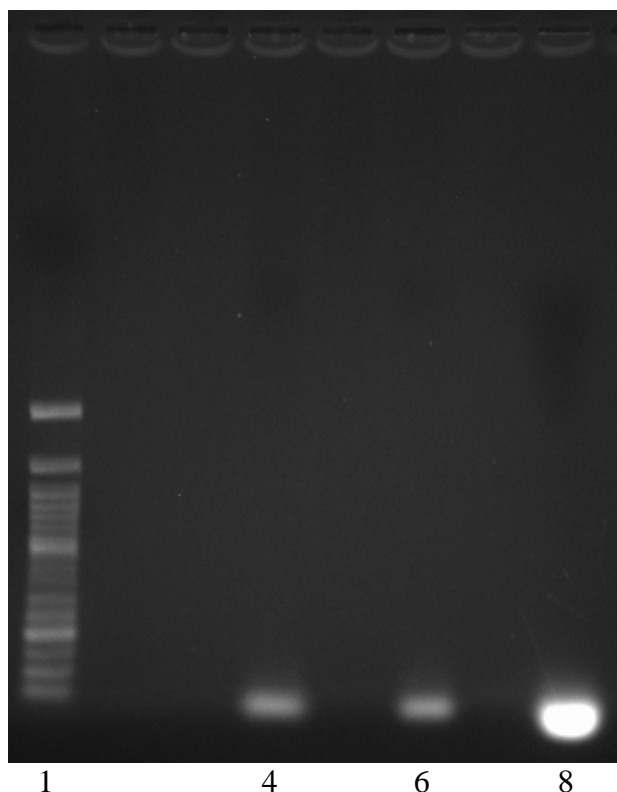


Figure 3-18. Fluorescence Image of Low Concentration Colloidal Gold Samples. Fluorescence photograph of 1% agarose gel demonstrating difference between Au-dT₂₀-dA₂₀ (lane 4) and Au-DSP-dT₂₀-dA₂₀ (lane 6) in reference to free duplex dT₂₀-dA₂₀ (lane 8).

Another gel was run with five times the colloidal gold by increasing the amount of colloidal gold from 200 μ L to one milliliter to bind with twice the number of oligonucleotides (20 nanomoles of dT₂₀) yielding a ratio of 1900 oligonucleotides/nanoparticle). The lower loading concentration demonstrated similar behavior to the previously discussed gel at twice the loading concentration. Figure 3-19 is a picture of the gel in the gel apparatus where the colloidal gold samples are clearly visible. Lane one

of Figure 3-19 is the 50 base pair ladder with tracking dye. The second lane, a colloidal gold control, demonstrated minimal migration and clusters that failed to enter the gel. This was as expected because there are but a few weakly charged citrate ions bound to the gold nanoparticle to give it mobility.

Lanes three and four, Au-dT₂₀ and Au-dT₂₀-dA₂₀ respectively, demonstrate a distinctive blue tint which indicates clusters of nanoparticles and displays a large distribution of mobility. AFM measurements on colloidal gold in section 3.1.2 confirm the tendency of colloidal gold to form large clusters in comparison to that of Au-DSP-dT₂₀.

The modified colloidal gold samples, Au-DSP-dT₂₀ and Au-DSP-dT₂₀-dA₂₀ (lanes 5 and 6 respectively) demonstrated relatively uniform mobility that clearly outpaced the mobility of the oligonucleotide adsorbed on gold (Au-dT₂₀) and the oligonucleotide duplex adsorbed on gold (Au-dT₂₀-dA₂₀). Literature has noted that thiol-bound oligomers to colloidal gold migrate 12 times faster than colloidal gold alone.¹⁷ It has been noted elsewhere that the difference in mobility between nonspecifically adsorbed oligonucleotide and bound oligonucleotide can be attributed to a difference in binding geometry.^{17, 18} The oligonucleotide adsorbed on gold adopts a lying down orientation that adds little to the size of the nanoparticle while the oligonucleotide bound to gold through the DSP coupling reagent assumes an upright orientation. The significant aggregation of the adsorbed oligonucleotide, much of which failed to enter the gel, proved to be a greater factor in determining the mobility as opposed to the binding geometry. Instead, separation of oligonucleotide adsorbed on gold was based largely on

particle size generating a large smear for both dT₂₀ adsorbed on gold and dT₂₀-dA₂₀ adsorbed on gold.

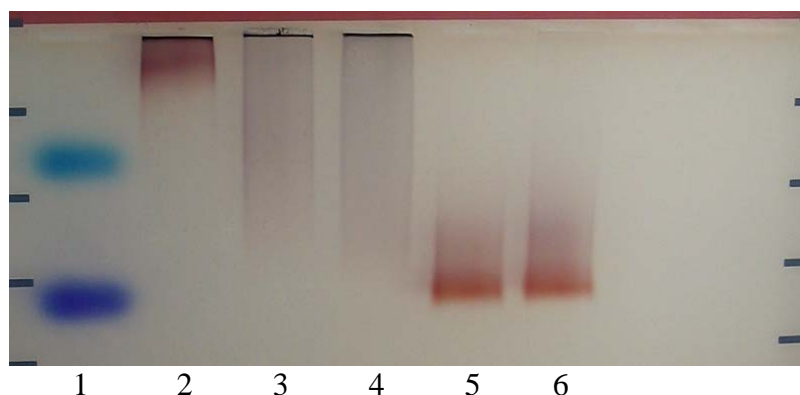


Figure 3-19. Gel Electrophoresis of High Concentration Colloidal Gold Samples. Photograph of 1% agarose gel demonstrating difference between Au-dT₂₀-dA₂₀ (lane 4) and Au-DSP-dT₂₀-dA₂₀ (lane 6) in reference to colloidal gold (lane 2).

Fluorescence imaging of the gel pictured in Figure 3-20 displays both the excess duplex shown as bright spots, and dark spots attributed to the absorption of UV by colloidal gold in lanes 2-6. Migration of the free duplex (lane 8) displays roughly the same intensity and patterning observed in Figure 3-18. The free duplex in lane eight appears to display an intensity that is roughly twice that of the bound duplex in lanes four and six. It's possible that this sample formed a duplex by reacting with excess DSP in solution resulting in twice the molecular weight observed in the other samples.

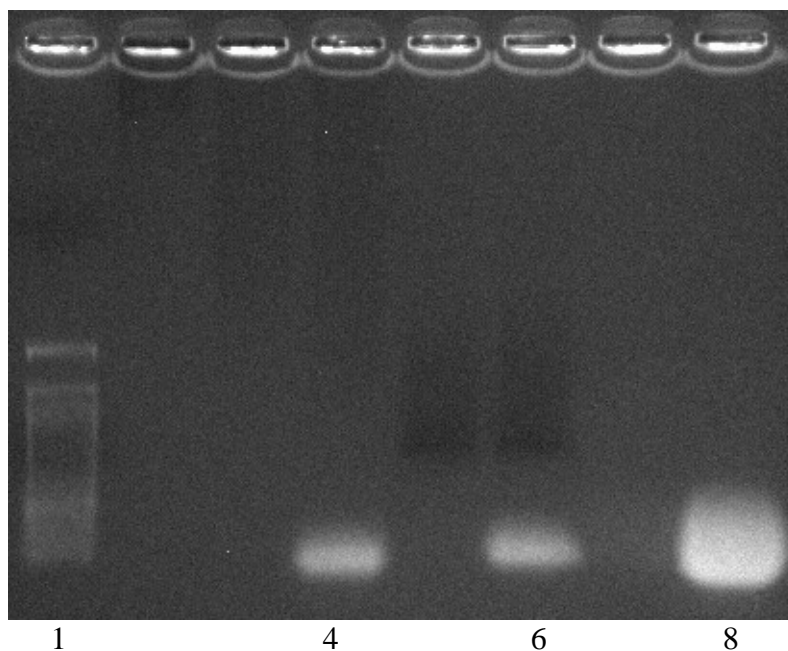


Figure 3-20. Fluorescence Image of High Concentration Colloidal Gold Samples. Fluorescence photograph of 1% agarose gel demonstrating difference between Au-dT₂₀-dA₂₀ (lane 4) and Au-DSP-dT₂₀-dA₂₀ (lane 6) in reference to free duplex (dT₂₀-dA₂₀) (lane 8).

3.1.7 Microgravimetry by Quartz Crystal Microbalance

The red trace of Figure 3-21 is a typical QCM response seen for the deposition of DSP onto a gold sensor surface. A negative change in oscillating frequency indicates that the sensor surface is slowing down as a result of mass developing on the sensor surface. An average of five runs resulted in 119 ± 4.07 ng of DSP bound to the sensor surface of 20.4 mm^2 . Expressing the same data as a molar amount of DSP bound as a function of area yields 14.5 pmol/mm^2 of DSP (29.0 pmol/mm^2 of the DSP fragment). These results appear to be high when compared to the predicted values from molecular modeling (6.67 pmol/mm^2). However, the surface roughness of the vapor deposited gold on quartz, not accounted for in these calculations, will add significantly to the surface area. The blue trace overlaid onto the deposition curve of DSP in Figure 3-21 is a control demonstrating that the addition of solvent fails to contribute to an increase in mass on the sensor surface.

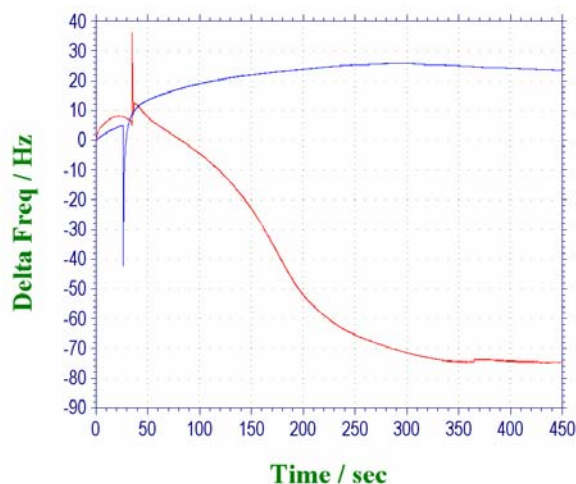


Figure 3-21. QCM Plot of Au-DSP. QCM curves demonstrating deposition of DSP in DMF(red) to inactivity of a DMF control(blue).

While the amount of DSP bound to the sensor surface displayed a surprisingly low standard deviation, saturation times of the QCM surface ranged from 300-1300 seconds. This rather large range is suspected to originate from slight inconsistencies in the cleaning procedure. Literature sources also reflect the uncertainty of SAM binding kinetics. Grubor and Shinar claim that saturation of a gold surface is “reached within about 5 min” for DSP, while other sources cite saturation times of 30 minutes or two hours.^{19, 22, 25}

With the DSP saturated electrode surface characterized, the immobilization of primary amine species by conjugation with DSP can be investigated. As previously noted, for the reaction of a primary amine with DSP to proceed efficiently, pH must be in the range of 7.5 - 8.5 which was achieved through the use of a HEPES buffer.^{22, 29, 30} A blank injection of solvent (DMF) was utilized as a control to demonstrate inactivity of the solvent with the DSP coated gold electrode at pH 8.0. The first injection of Figure 3-22 demonstrates an initial mass gain with the addition of 10 μ L of solvent but fails to demonstrate a gain in mass beyond the injection. The second injection demonstrates the

same spike attributed to a sample injection but, makes a second jump of approximately 200 ng attributed to binding of *n*-*boc*-1,4-phenylene diamine. Characteristic of both injections is the oscillating drift in baseline that suggests a loss in mass on the sensor surface over time. Whether this is hydrolysis of the DSP layer, rearrangement of the SAM, an inherent property of QCM as Alfonta noted or some other mechanism is unclear.¹⁹

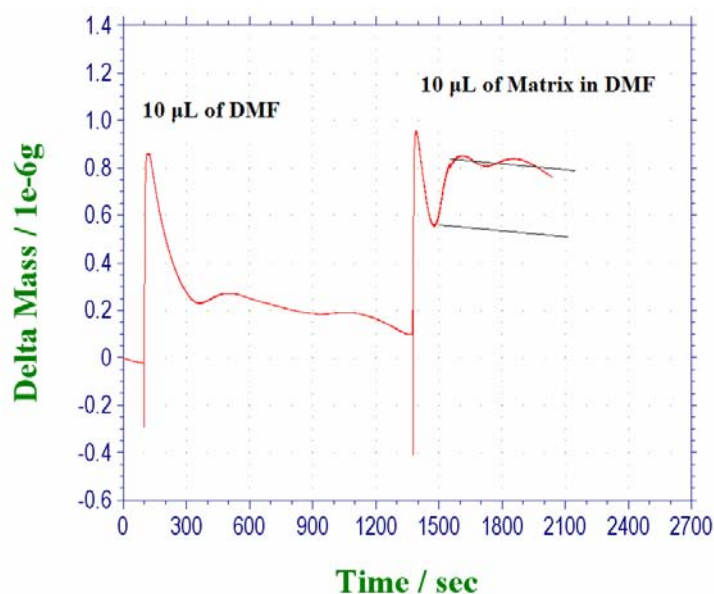


Figure 3-22. QCM Plot of Au-DSP-Matrix. Injection of a solvent blank over DSP surface followed by a 1 mM *n*-*boc*-1,4-phenylene diamine injection at pH of 8.0. Lines are drawn over the trace to indicate deposition of matrix.

The amount of *n*-*boc*-1,4-phenylene diamine attached to the surface can be determined as done with the deposition of DSP. The mechanism for attachment of *n*-*boc*-1,4-phenylene diamine involves the loss of the succinimidyl group on DSP to bind with the primary amine in a 1:2 relation. The reaction of DSP with *n*-*boc*-1,4-phenylene diamine yields a net gain in molar mass of:

$$\text{Matrix} - \text{NHS} = 208.26 - 114.09 = 94.17 \text{ g / mol}$$

or

$$\text{Matrix} + (\frac{1}{2} \text{DSP} - \text{NHS}) = 208.26 + (202.2 - 114.1) = 296.4 \text{ g / mol}$$

The reasoning for approaching this calculation two different ways will be apparent shortly. Converting the average change in mass on the sensor surface of multiple runs to a relation of moles per area for the reaction yields:

$$1.7_5(\pm 0.3_5) \times 10^{-7} \text{ g} \left(\frac{\text{mol}}{94.17 \text{ g}} \right) \left(\frac{1 \times 10^{12} \text{ pmol}}{1 \text{ mol}} \right) \left(\frac{1}{20.4 \text{ mm}^2} \right) = 91 \pm 18 \frac{\text{pmol}}{\text{mm}^2}$$

or

$$1.7_5(\pm 0.3_5) \times 10^{-7} \text{ g} \left(\frac{\text{mol}}{296.4 \text{ g}} \right) \left(\frac{1 \times 10^{12} \text{ pmol}}{1 \text{ mol}} \right) \left(\frac{1}{20.4 \text{ mm}^2} \right) = 29 \pm 6 \frac{\text{pmol}}{\text{mm}^2}$$

Calculating surface density of the conjugate by the first pathway yields a ratio that is four times what's possible for occurring with the determined monolayer of DSP. The second procedure suggests that the SAM of DSP dissociates from the surface with the formation of the DSP- *n*-boc-1,4-phenylene diamine conjugate and then redeposits. If a surface can break bonds to achieve a proper electron configuration, as discussed in section 1.2.2, maybe this is the mechanism for SAM rearrangement considering it yields the ideal 1:1 ratio. Another hypothesis for the high mass readings is thought to be the SAM of conjugate interacting with NHS and excess *n*-boc-1,4-phenylene diamine in solution. Experimental attempts to prove pi-pi and hydrophobic interactions of the SAM with species in solution by trying to bind lower concentrations of *n*-boc-1,4-phenylene diamine demonstrated imprecise results related to the inherent drift of the baseline previously described.

Efforts to demonstrate binding of primary amine labeled dT₂₀ to the DSP coated surface proved a difficult endeavor. Even though the gain in mass is quite substantial for even a single binding event (6100 g/mol) the sensor was incapable of resolving a change

in mass from the baseline drift. Figure 3-23 displays a typical plot for the reaction of a DSP coated surface with dT₂₀.

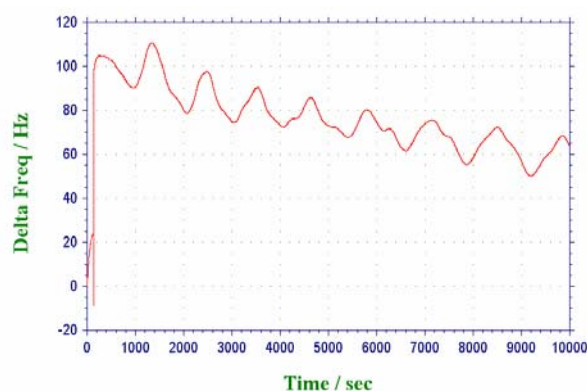


Figure 3-23. QCM Plot of Au-DSP-dT₂₀. QCM measurement of dT₂₀ oligomer deposition through DSP.

Oscillation of the QCM trace following an injection of dT₂₀ was substantially higher than what was seen for the *n*-*boc*-1,4-phenylene diamine. Whether this is suggestive of rearrangement of the SAM is unclear.

3.1.8 Electrochemistry

Cyclic voltammetry was used to study the oxidative/reductive potential of a species attached to an electrode. For these experiments, QCM electrodes were used as a working electrode with an area that is well defined (20.4 mm²) and consistent.

The first comparison made was between a control electrode and one coated with DSP. The bare gold electrode of the control failed to illicit a measurable response in the working range of 0.5 V to -0.2 V while the DSP coated electrode gave peak currents at -0.043 V and 0.17 V. The first cathodic scan of the DSP coated electrode yielded Figure 3-24.

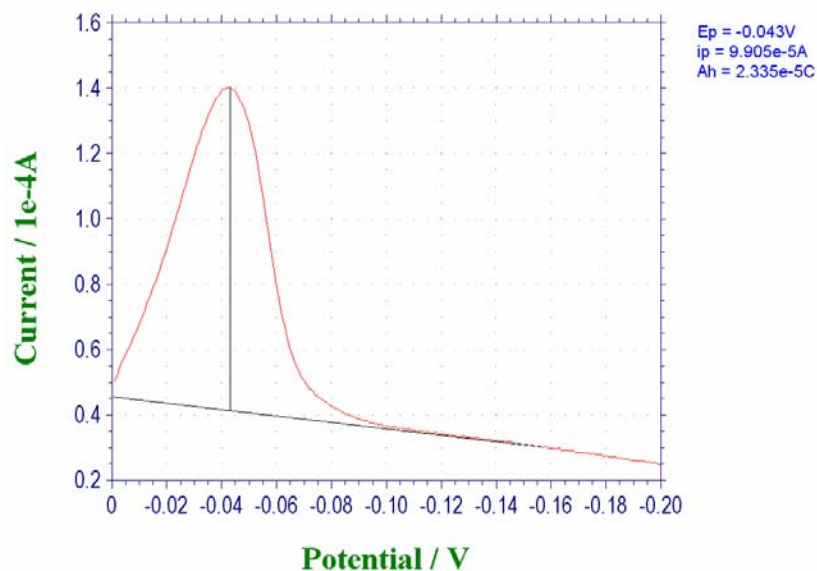


Figure 3-24. Voltammogram of Au-DSP. Initial cyclic voltammetric scan of a DSP coated surface.

Realizing that when an electrochemically active species is confined to the surface of an electrode, the number of moles is simply the number of coulombs divided by Faraday's constant and the number of electrons transferred per mole.

$$\# \text{ moles} = \frac{2.335 \times 10^{-5}}{9.649 \times 10^4} = 2.42 \times 10^{-10}$$

Expressing this result as a function of electrode geometric area gives 11.9 pmol/mm² of the DSP fragment on the electrode surface. The number of moles per unit area is lower than what was observed with QCM results (29.0 pmol/mm² for the DSP fragment) which may indicate that only a third of the DSP is accessible to the surface.

Next in the series was to perform cyclic voltammetry on a SAM of *n*-boc-1,4-phenylene diamine linked to an electrode surface through DSP. The two peaks observed in the SAM of DSP, at -0.04 V and 0.17 V, are apparent along with a new pair at approximately 0.18 V and 0.28 V (Figure 3-25). The peak area associated with DSP is

approximately ten times less than what was observed for the DSP sample suggesting a dramatic decrease in this species.

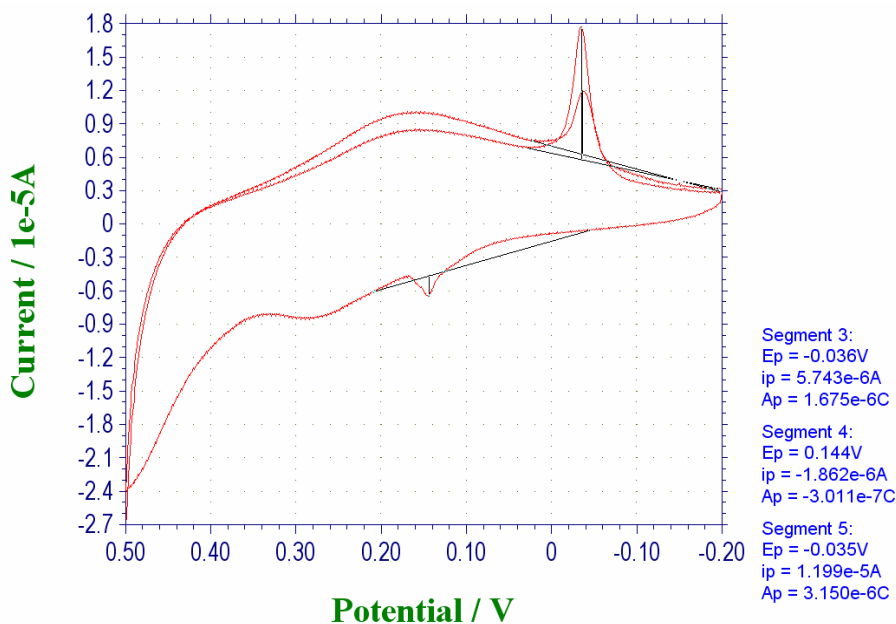


Figure 3-25. Voltammogram of Au-DSP-Matrix. Voltammogram displaying decrease in peaks observed in DSP sample with addition of *n*-boc-1,4-phenylene diamine surface.

The final SAM under evaluation was the DSP-dT₂₀ coated surface with remaining sites occupied by *n*-boc-1,4-phenylene diamine. With this sample came a complete loss in activity of the surface as displayed by Figure 3-26. Results for the dT₂₀ coated surface are comparable to the bare gold control electrode indicating no activity for DSP.

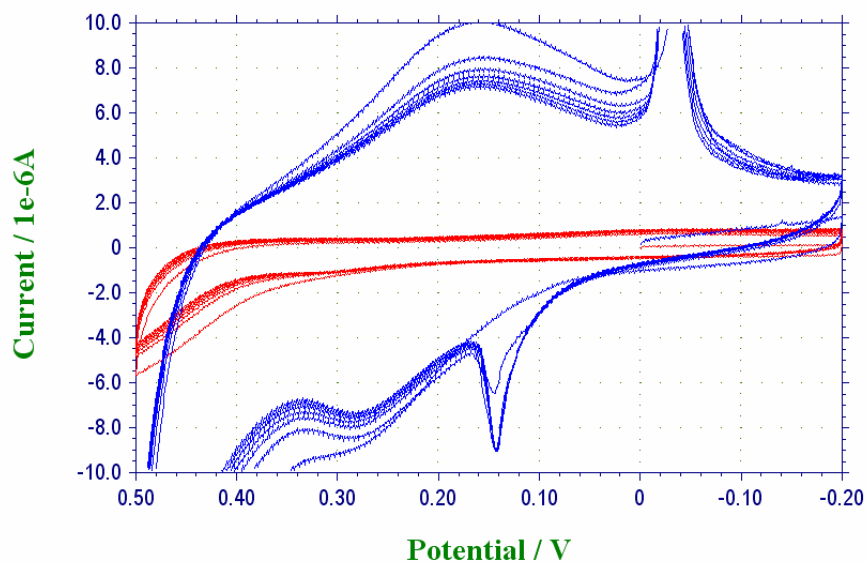


Figure 3-26. Voltammogram of Au-DSP-dT₂₀. Cyclic voltammogram overlay of DSP-Matrix (blue) from Figure 3-25 to DSP-dT₂₀ (red).

The redox behavior of a modified electrode in contact with the electroactive $\text{Fe}^{\text{III}}(\text{CN})_6^{3-} / \text{Fe}^{\text{II}}(\text{CN})_6^{4-}$ redox couple was also measured by monitoring the drop in peak current as a result of an increase in the diffusion layer thickness.

A control gold electrode was prepared in a similar manner to the SAM coated gold electrodes of section 2.2.7. Cyclic voltammetry of a 1 mM solution of $\text{K}_4\text{Fe}(\text{CN})_6$ with a control electrode of area 1.3 cm^2 gave the results in Figure 3-27.

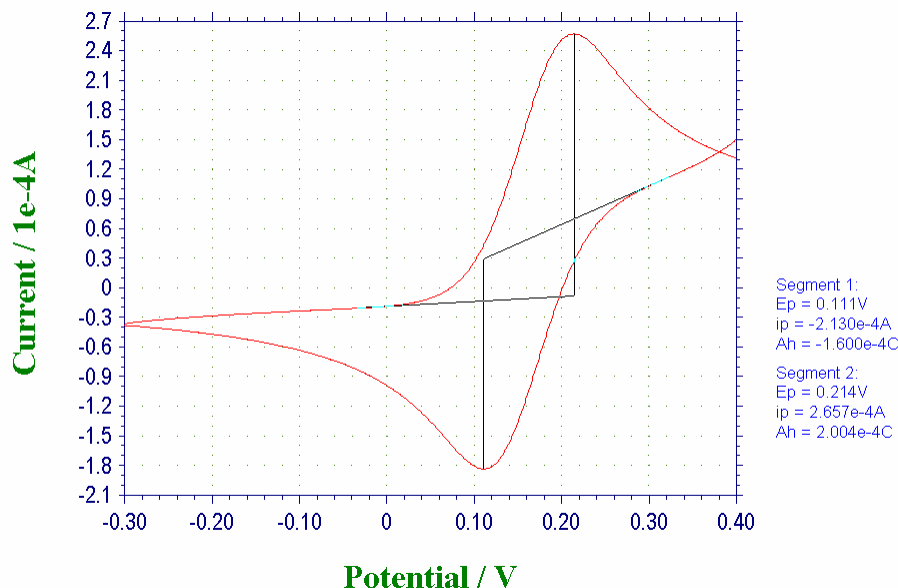


Figure 3-27. CV of Gold Electrode. Cyclic voltammogram of control electrode in a 1 mM solution of $\text{K}_4\text{Fe}(\text{CN})_6$.

Applying the Randles-Sevcik equation to the control voltammogram and solving for concentration gives:

$$\frac{2.66 \times 10^{-4} \text{ A}}{(0.1 \text{ V} / \text{s})^{1/2}} = (2.69 \times 10^5 \text{ C} / \text{mol})(1e^-)(1.3 \text{ cm}^2)(1.96 \times 10^{-5} \text{ cm}^2 / \text{s})^{1/2} C$$

$$C = 5.5 \times 10^{-7} \text{ mol} / \text{mL} = 0.55 \text{ mM}$$

The actual concentration of $\text{K}_4\text{Fe}(\text{CN})_6$ in solution was 1 mM. Because the concentration of the supporting electrolyte was 0.1 M, the activity coefficient for $\text{Fe}^{\text{II}}(\text{CN})_6^{4-}$ is 0.2 which results in an activity of 0.20 mM. The calculated results are 0.55/.2 higher than theoretical which suggests that the true surface area (not the geometric surface area) of the electrode is 3.6 cm^2 . There is also a deviation from ideal when examining the difference in redox potential (ΔE_p) for the reversible couple $\text{Fe}^{\text{III}}(\text{CN})_6^{3-} / \text{Fe}^{\text{II}}(\text{CN})_6^{4-}$.

$$\Delta E_p = E_{pa} - E_{pc} = 0.214 - 0.111 = 0.103$$

Considering that the reaction is a single electron transfer the difference in the peak anodic and peak cathodic current should be close to 0.059 V. Applying an IR compensation value brings the difference in redox potential closer to the ideal. Deviations from the ideal might be indicative of a slow electron transfer at the electrode surface.⁵¹ However what is more likely is that at the scan speed employed, ΔE_p becomes larger than expected.

A DSP coated electrode, handled in the same manner as the control, demonstrated far lower responses for peak current along with a shift in potential suggesting that $K_4Fe(CN)_6$ in solution was diffusion inhibited by a SAM of DSP.

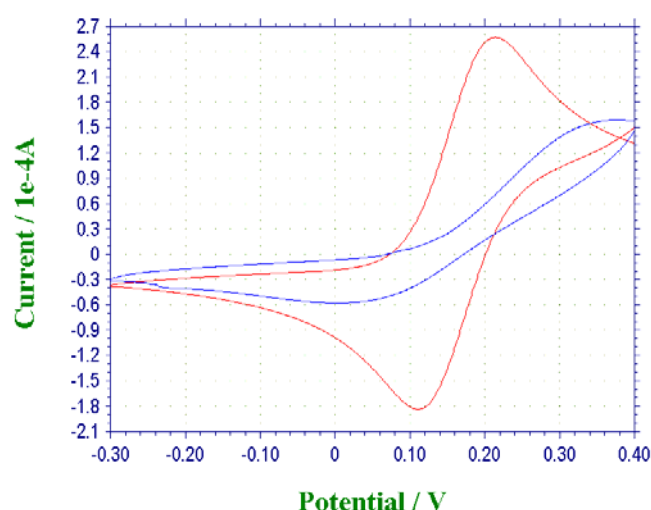


Figure 3-28. CV of Au-DSP. Cyclic voltammogram of a control electrode(red) overlaid with DSP coated electrode(blue) demonstrating diffusion impedance.

Another monolayer under evaluation was whether the amine group or another functional group of *n*-boc-1,4-phenylene diamine was binding to the gold surface. Figure 3-29 demonstrates that *n*-boc-1,4-phenylene diamine does not bind to the gold surface directly since there is no change in the peak current from the control. Also plotted on the same graph is the response from a DSP coated electrode exposed to a solution of *n*-boc-

1,4-phenylene diamine. There is a slight increase in the peak current along with a shift in potential from what was observed in the DSP coated slide of Figure 3-28.

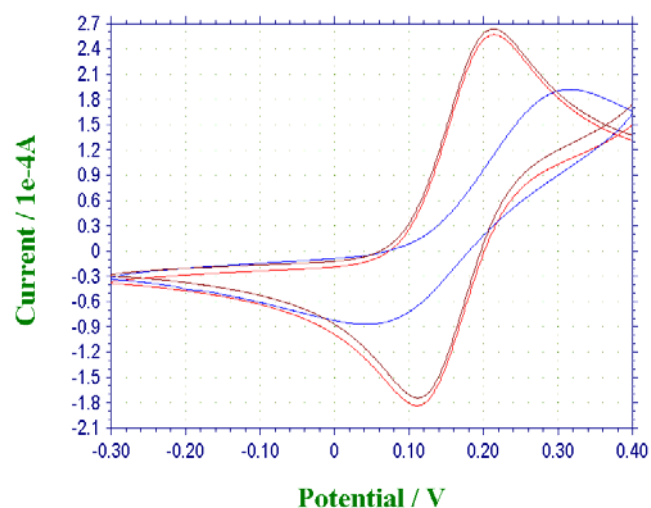


Figure 3-29. CV of Au-DSP-Matrix. Overlay of cyclic voltammograms of a control electrode(red), gold electrode exposed to *n*-*boc*-1,4-phenylene diamine(dark red) and DSP linked to *n*-*boc*-1,4-phenylene diamine coated electrode(blue).

The diffusion of $K_4Fe(CN)_6$ through a dT_{20} coated gold slide was a final study in this series. In a similar manner to *n*-*boc*-1,4-phenylene diamine samples, dT_{20} was exposed to a bare gold slide and a DSP coated gold slide. In both cases the peak current was substantially reduced over what was observed for the bare gold electrode suggesting that the oligonucleotide binds to the gold surface by electrostatic interactions or through DSP by a terminally labeled primary amine on the oligomer. Of interesting note, the slide with dT_{20} adsorbed to the surface appears to have restricted migration more than the SAM of DSP bound to dT_{20} . This could be an indication of the lying down phase of adsorbed oligomer in comparison to the upright phase of DSP bound oligomer.

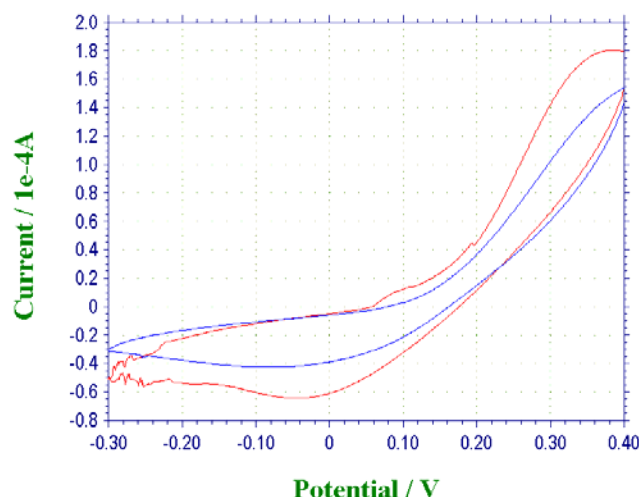


Figure 3-30. CV of Au-DSP-dT₂₀ and Au-dT₂₀. Overlay of cyclic voltammograms of bare gold electrode exposed to oligomer (blue) and oligomer linked to the electrode surface through DSP (red).

3.1.9 Surface Plasmon Resonance

As demonstrated with previous SAM experiments, the first step in SPR measurements was to determine the amount of DSP bound to the sensor surface as a function of area. The degree of DSP deposition was determined by acquiring a SPR measurement of both flow cell 1 (Fc₁) and flow cell 2 (Fc₂) of the functionalized surface and subtracting values collected from a freshly cleaned sensor. An increase in response units, or shift in refractive index, indicates an attachment of DSP to the surface. Since one response unit is equivalent to 1 pg/mm² (as determined by Biacore) and the instrumental limits are for species >180 g/mol it should be possible to determine the amount of DSP bound as a function of area. Attempts at demonstrating binding of DSP displayed inconsistent results most likely attributed to the experimental procedure. A valid approach to demonstrating binding, as the SPR instrument is designed, would be to flow a solution of DSP in either DMSO or DMF over a freshly cleaned sensor surface while mounted in the instrument. However, the effects of high concentrations of DMSO

or DMF on the instrument were unknown which led to performing deposition steps for DSP off-line from the instrument which yielded inconsistent results.

Following the formation of a SAM of DSP studying the immobilization of dT₂₀ was the next step. With the 100 nM of oligomer suspended in HEPES buffer there were few concerns regarding compatibility issues with the instrument which allowed binding to be studied in real time. Multiple injections of 100 μ L of 100 nM dT₂₀ at a flow rate of 10 μ L/min were performed to establish a binding rate. An initial response generated a gain of 16 response units followed by five sequential injections generating responses of 9.57 ± 0.16 response units per injection (Figure 3-31).

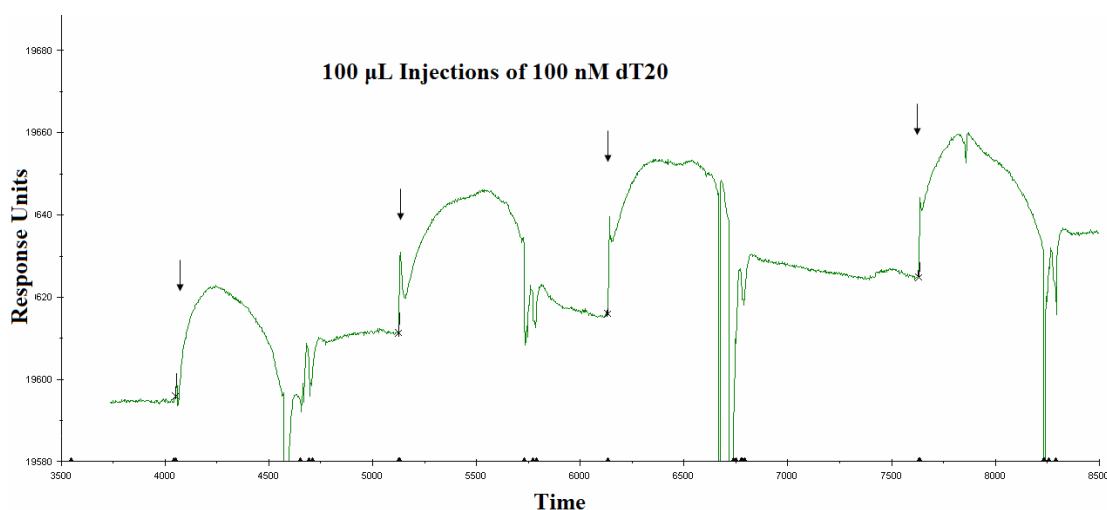


Figure 3-31. SPR Plot of Au-DSP-dT₂₀. Immobilization of dT₂₀ onto SPR gold sensor surface through DSP with injection points marked by arrows.

Saturation of the surface with dT₂₀, under these conditions, appears to occur at 150 ± 10 response units which convert to 0.024 pmol/mm^2 . Saturation was determined to occur with no increase in signal and a degradation of the peak curve following injection as demonstrated by the saturating trend seen in the first three injections of Figure 3-31. The first injection demonstrates a relatively consistent arc throughout the injection with a shift in baseline following a wash step. The following two injections of dT₂₀ display an

increasing radius arc with minimal change in baseline indicating no additional binding was occurring. While the surface was determined to be saturated with dT₂₀, it was still possible to bind *n*-boc-1,4-phenylene diamine. Injections four through eight marked by red arrows in Figure 3-32, 100 μ L of 10 μ M *n*-boc-1,4-phenylene diamine, demonstrate an increase with each injection of 38 ± 5 response units or 0.18 pmol/mm^2 . The final 100 μ L injection of 100 nM dT₂₀ serves as verification that the surface is still inactive to dT₂₀.

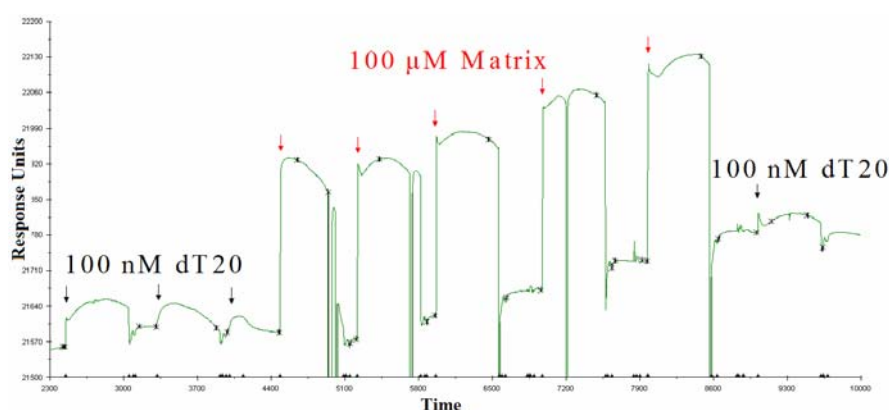


Figure 3-32. SPR Plot of Au-DSP-Matrix. Immobilization by way of DSP of *n*-boc-1,4-phenylene diamine (matrix) onto a dT₂₀ saturated surface.

Comparing the surface density of dT₂₀ to a maximum density for efficient hybridization as reported by either Castellino or Peterlinz of $0.04 \text{ molecules/nm}^2$ and $0.052 \text{ molecules/nm}^2$ requires a conversion of units.^{53, 58}

$$150 \frac{\text{pg}}{\text{mm}^2} \left(\frac{1 \times 10^{-12} \text{ g}}{\text{pg}} \right) \left(\frac{\text{mol}}{6201 \text{ g}} \right) \left(\frac{6.022 \times 10^{23}}{1 \text{ mol}} \right) \left(\frac{\text{mm}}{10^6 \text{ nm}} \right)^2 = 0.015 \text{ molecules / nm}^2$$

According to the literature, at a density of $0.015 \text{ molecules/nm}^2$ for dT₂₀ it should be possible to achieve nearly 100% hybridization. Experiments have established that with three 10 μ L injections of 10 μ M dA₂₀ the signal gain jumps to 145 response units which

translates to 0.023 pmol/mm² or 97% hybridization. The Sips model can be utilized in predicting bound target coverage (Γ_{target}) which can be compared to experimental results.

$$\Gamma_{target} = \Gamma_{max} \frac{(K_A \times c)^a}{1 + (K_A \times c)^a}$$

Applying an equilibrium binding constant for the formation of the duplex (K_A) of $1.8 \times 10^7 \text{ M}^{-1}$ obtained from Corn and coworkers, assuming Langmuir adsorption so that the binding energy (a) is one, and substituting the concentration (c) for dA₂₀ of 10 μM then it is possible to solve for the relation.⁶⁷

$$\Gamma_{target} = \Gamma_{max} \times 0.994$$

The Sips model predicts that approximately 99% of available sites should be occupied under stop-flow conditions which is close to the experimentally determined value of 97% hybridization under flowing conditions.

To demonstrate specificity, a sequence of non-compliment DNA (ncDNA) was added at the same concentration as dA₂₀. As expected, the ncDNA displayed no interaction with the dT₂₀ coated sensor surface while interspersed injections of dA₂₀ demonstrated hybridization across both flow cells (Figure 3-33).

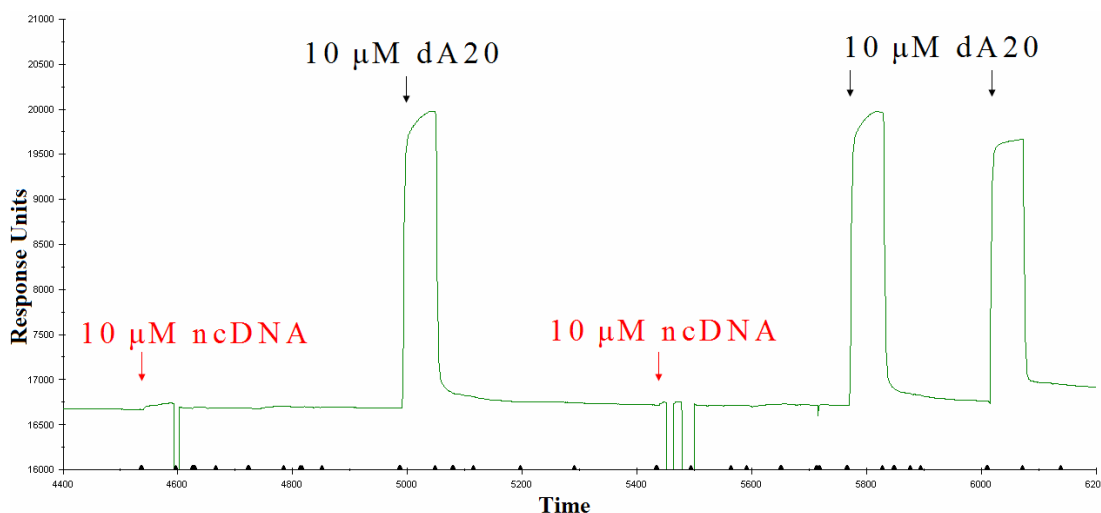


Figure 3-33. SPR Plot of Au-DSP-dT₂₀-dA₂₀. Hybridization of dT₂₀ coated surface with dA₂₀ and inactivity with non-compliment DNA (ncDNA) for Fc₁ and Fc₂.

3.2.0 MALDI-TOF Mass Spectrometry

Initial MALDI experiments based on the formation of a SAM of oligonucleotide bound through DSP were basic in design. The intent was to gain a general understanding of what to expect from the formation of a SAM on gold. With the knowledge of what to expect from the background generated by the components of the assay and instrument set-up then finding an optimal configuration of a SAM can be pursued.

The first experiment focused on the assembly of a monolayer of oligonucleotide on a gold substrate. A gold MALDI target plate was used as a foundation to explore the differences between oligomers immobilized through physisorption and chemisorption (Table 2-1). Controls were also set-up to elucidate the background signal attributed to the gold plate, assay components and the single stranded oligomer dT₂₀. Upon laser desorption ionization, the gold plate control sample (A1) produced gold clusters, some with attached chlorine with little else appearing in the spectrum. These results suggest that DMF and the components of the HEPES buffer add little to the background of the spectrum. No significant difference was noted with the ss dT₂₀ adsorbed on gold control

sample (B1) but, with the adsorbed duplex sample, dT₂₀-dA₂₀ (C1), a shift in background in the low mass range was observed. Unfortunately, there was no indication of the molecular ion peak associated with the adsorbed duplex. The remaining samples of the experiment utilized DSP to immobilize oligomer to the gold plate. Surprisingly, the signal intensity for the gold clusters jumped significantly for samples Au-DSP- dT₂₀ (D1) and Au-DSP- dT₂₀-dA₂₀ (E1) along with the formation of a new peak attributed to sulfur (+32) attached to gold. However, the molecular ion peak for dA₂₀ was still absent from the mass spectrum.

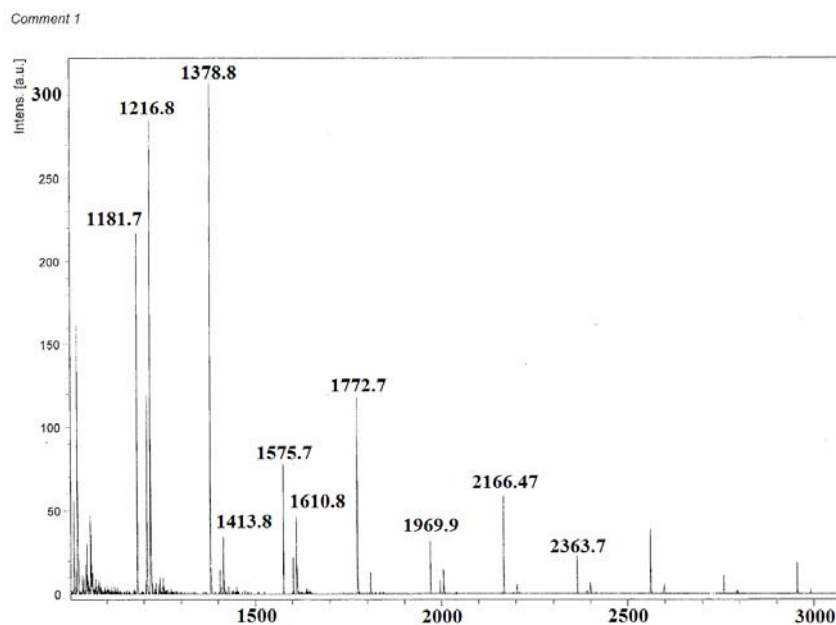


Figure 3-34. MALDI Spectra of Au. MALDI spectra from gold plate (A1) displaying aggregates of Au along with adducts of chlorine.

With the results of the first experiment not yielding the molecular ion peak it was thought that the matrix, *n*-*boc*-1,4-phenylene diamine, needed to be added and the correct ratio of matrix to oligonucleotide determined. A second experiment was designed to

cover a range of (ds) oligonucleotide concentrations within a mixed SAM of (ds) oligonucleotide and matrix with the hope of generating a molecular ion peak for dA₂₀. On a spot size of roughly 2.5 mm in diameter, having an area of 4.9 mm², it is possible to determine a ratio of matrix to oligonucleotide. Knowing the molar amount of dT₂₀ added to the plate from Table 2-2 the density range is from 41 pmol/mm² to 41 fmol/mm². As demonstrated from QCM experiments, the maximum density of DSP on the surface is 29 pmol/mm² which means the gold surface will likely be saturated with oligonucleotide. From SPR experiments, it was mentioned that a maximum density for efficient hybridization was in the range of 0.04 molecules/nm² or 0.052 molecules/nm².^{53, 58} Converting the density units to molecules/nm² gives a maximum possible range of 25 to 0.025 molecules/nm². The ultimate goal of varying the concentration of oligonucleotide was to determine a functional ratio of matrix to analyte. With density concentrations of fmol/mm² for the oligomer then there would be a ratio of roughly 1:1000 (analyte: matrix). Results paralleled what was observed in the first set of MALDI experiments. For oligonucleotides bound to gold through DSP, intense peaks were observed for the gold clusters and gold clusters with attached sulfur. Peaks for gold had displayed a mass shift of three for samples with DSP which could be the addition of hydrogen as seen in ¹H NMR samples. Interestingly, the dual SAM of matrix and oligonucleotide generated minimal signal intensities across the range of oligonucleotide densities.

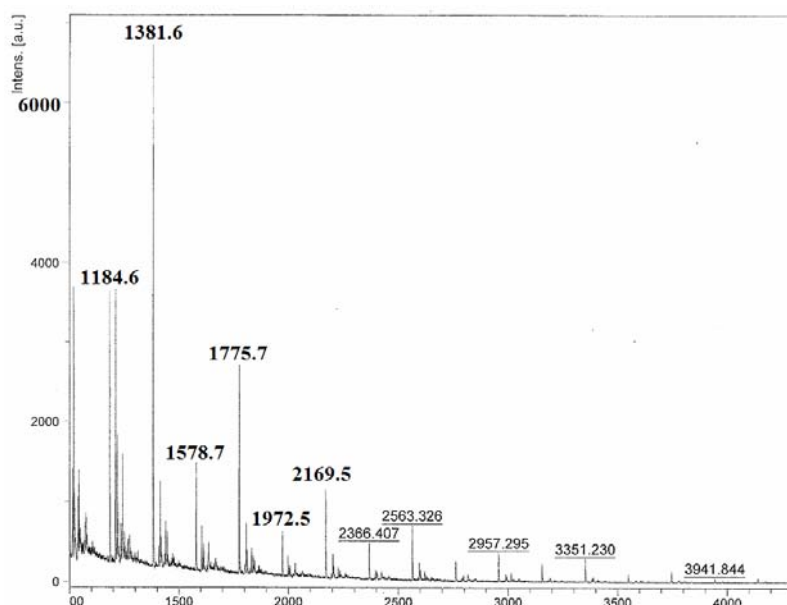


Figure 3-35. MALDI Spectra of Au-DSP-Matrix. MALDI spectra from a SAM of DSP-Matrix (B2) displaying aggregates of Au at a higher intensity in the presence of DSP along with a mass shift of three.

A third experiment focused on immobilizing oligonucleotide to a gold MALDI target plate and adding colloidal gold with different functionalities. Table 2-3 displays the numerous variations of SAMs on the MALDI plate in combination with SAMs on colloidal gold. This time the use of Tris was employed in the mixed SAM on the MALDI plate. UV-Vis absorption experiments demonstrated how tris generated gold particles with sufficient charge to break apart aggregation. It was thought by applying tris to the underlying surface of the MALDI plate it would ensure that the oligonucleotides would adopt a more upright phase, given their negative charge, than what would be achievable by matrix or DSP. Colloidal gold served as a matrix either neat or functionalized with DSP bound *n*-*boc*-1,4-phenylene diamine. Even with the varied sample configurations a similar mass spectrum was generated. However, this time additional peaks appeared not present in the previous experiments. With the addition of colloidal gold to the surface a final rinse of the surface with distilled water was not possible this meant components of

the HEPES buffer system were present on the plate. Peaks for the buffer components of Na_2HPO_4 (141), HEPES (239), HEPES + Na (260) appear throughout the sample batch. Peaks for gold had displayed a mass shift of 2 which could be the addition of hydrogen as seen in ^1H NMR samples. Also apparent are peaks which could be attributed to adducts attached to gold appearing 26 or 28 m/z above the peaks ascribed to gold (Au-H_2+26 or $\text{Au}+28$). These appear at 226.4, 423.8, and 622.1.

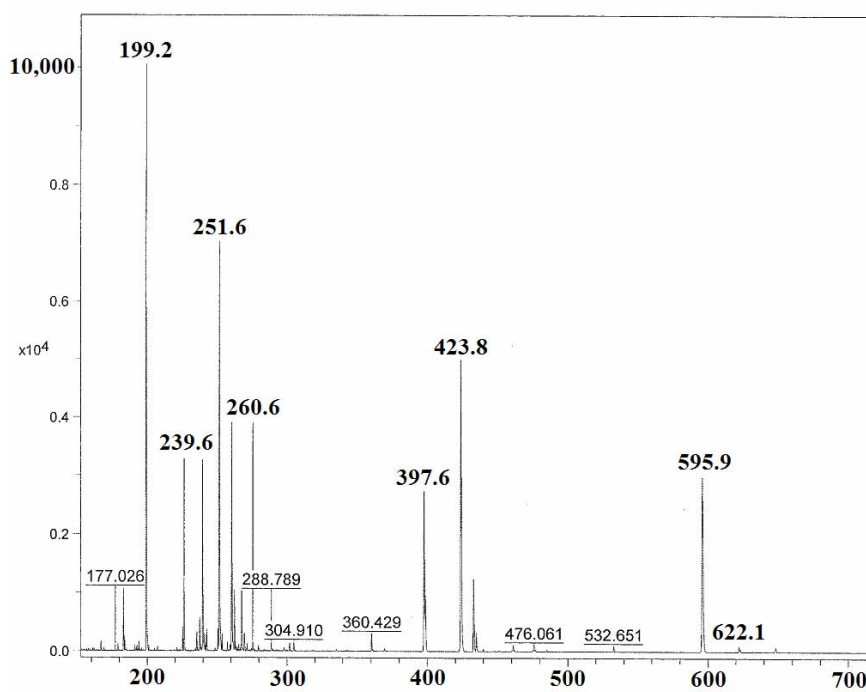


Figure 3-36. MALDI Spectra of Mixed SAM. MALDI spectra from adsorbed duplex mixed with colloidal gold (I3) displaying aggregates of Au at a higher intensity in the presence of DSP along with a mass shift of two.

CHAPTER 4.0

CONCLUSIONS

4.1.0 Discussion of Analytical Results

Characterization of the formation of a SAM by orthogonal analytical techniques has led to a defined surface. Each step in the formation of a SAM, from deposition of DSP to hybridization with the immobilized oligomer, was demonstrated by several analytical techniques. Molecular modeling demonstrated a theoretical value of 6.67 pmol/mm² for DSP on an atomically flat Au (1,1,1) surface. It was demonstrated that a vapor deposited gold surface is capable of binding 14.5 pmol/mm² of DSP by QCM and 11.9 pmol/mm² by electrochemical methods. For colloidal gold it was determined by UV-Vis that a maximum surface density prior to aggregation is reached at 2.8 pmol/mm². Confirmation of forming the amide, between DSP and a primary amine, was clearly demonstrated by IR and NMR spectra. QCM and electrochemical measurements suggested nearly complete substitution of the NHS ester of DSP with *n*-*boc*-1,4-phenylene diamine. Immobilization of the dT₂₀ probe was demonstrated by SPR, gel electrophoresis, and cyclic voltammetry. The final step of hybridization was demonstrated by SPR and gel electrophoresis.

Distinctive features of a SAM were observed in the course of characterization measurements. The large oscillations observed in QCM measurements suggest

rearrangement of the monolayer (section 1.2.2). The geometrical phases of the oligomer are apparent in cyclic voltammetry and gel electrophoresis experiments. In cyclic voltammetry the adsorbed species, striped phase, retarded migration of the electrochemically active species more than the upright phase of DSP linked oligonucleotide. Migration rates in gel electrophoresis displayed faster migration for the adsorbed duplex which supports the idea of a striped phase since the charge increases with little change in hydrodynamic drag. The opposite is true for the DSP linked oligonucleotide in gel experiments where the formation of the complement in an upright phase resulted in a significant increase in the hydrodynamic drag.

The aggregate nature of colloidal gold was also substantiated by each analytical technique. AFM demonstrated that the size and shape of aggregates was a function of the applied SAM. Gel electrophoresis and UV-Vis demonstrated that a charge could be added to the surface (DSP-Tris at pH 8.0) to aid in migration and minimize aggregation.

Preliminary results for MALDI experiments have indicated that a DSP bound monolayer of *n*-boc-1,4-phenylene diamine promotes the formation of gold cluster ions but, fails to generate the molecular ion peak of the oligonucleotide. As Smith pointed out, the chemical differences between an effective or ineffective matrix are extremely subtle.⁴²

The choice of an immobilized matrix, *n*-boc-1,4-phenylene diamine, could prove to be an unlikely substitute for MMPC. Removal of the *t*-boc group, to give more of a resemblance to MMPC, might provide the necessary conditions for desorption and ionization for the production of the molecular ion. Future work might involve incorporation of formamide to melt the duplex and ease desorption. Excision of samples

from gel electrophoresis experiments and determining the amount of immobilized oligonucleotide, with the addition of KCN to free immobilized oligomer, could prove useful in determining a ratio of matrix to analyte. Establishing a surface roughness for the MALDI plate and other gold surfaces could also prove useful when determining an ideal ratio of matrix to analyte. The intent of creating a uniform SAM of matrix should prove invaluable upon finding an appropriate matrix.

REFERENCES

1. Hermanson, G. 1996. Bioconjugate Techniques. San Diego. Academic Press. Inc.
2. Hermanson, G. 1992. Immobilized Affinity Ligand Techniques. San Diego. Academic Press Inc.
3. Brockman, A.; Orlando, R. 1995. Probe-immobilized Affinity Chromatography/Mass Spectrometry. *Anal. Chem.* 67. pp. 4581-4585.
4. Siuzdak, Gary. 2003. The Expanding Role of Mass Spectrometry in Biotechnology. San Diego. MCC Press.
5. Silverstein, R.; Webster, F. and Kiemle, D. 2005. Spectrometric Identification of Organic Compounds. New York. Wiley.
6. Atkins, P.; de Paula, Julio. 2005. Elements of Physical Chemistry. New York. Oxford.
7. Atkins, P. Physical Chemistry. 1990. New York. W.H. Freeman and Company.
8. Adamson, A. 2000. The Solid-Liquid Interface: Adsorption from Solution. *Phys. Chem. of Surfaces*. 5. pp. 421-459.
9. Langmuir, I. J. Am. Chem. 1917. Constitution and Fundamental Properties of Solids and Liquids. *Soc.* 39. pp. 1848-1906.
10. Langmuir, I. J. Am. Chem. 1918. The Adsorption of Gases on Plane Surfaces of Glass, Mica and Platinum. *Soc.* 40. pp. 1361.
11. Rosen, M. 1978. Surfactants and Interfacial Phenomena. New York. John Wiley and Sons.
12. Schwartz, D. 2001. Mechanisms and Kinetics of Self-Assembled Monolayer Formation. *Phys. Chem.* 52. pp. 107-137.
13. Dubois, L.; Nuzzo, R. 1992. Synthesis, Structure, and Properties of Model Organic Surfaces. *Annu. Rev. Phys. Chem.* 43. pp. 437.

14. Bain, C.; Troughton, E.; Tao, Y.; Whitesides, G.; et. al. 1989. Formation of Monolayer Films by the Spontaneous Assembly of Organic Thiols from Solution onto Gold. *J. Am. Chem. Soc.* 111. pp. 321.
15. Hu, J.; Zang, J.; Liu, F. Kittredge, K. et. al. 2001. Competitive Photochemical Reactivity in a Self-Assembled Monolayer on a Colloidal Gold Cluster. *J. Am. Chem Soc.* 123. pp. 1464-1470.
16. Schreiber, F. 2004. Self-Assembled Monolayers: From 'Simple' Model Systems to Biofunctionalized Interfaces. *J. Phys.: Condens. Matter.* 16. pp. 881-900.
17. Sandström, P.; Boncheva, M.; Åkerman, B. 2003. Nonspecific and Thiol-Specific Binding of DNA to Gold Nanoparticles. *Langmuir.* 19. pp. 7537-7543.
18. Parak, W.; Pellegrino, T.; Micheel, C.; et. al. 2003. Conformation of Oligonucleotides Attached to Gold Nanocrystals Probed by Gel Electrophoresis. *Nano Lett.* 3. pp. 33-36.
19. Alfonta, L.; Willner, I. 2001. Electrochemical and Quartz Crystal Microbalance Detection of the Cholera Toxin Employing Horseradish Peroxidase and GM1-Functionalized Liposomes. *Anal. Chem.* 73. pp. 5287-5295.
20. Storri, S.; Santoni, T.; Minunni, M.; Mascini M. 1998. Surface Modifications for the Development of Piezoimmunosensors. *Biosensors & Bioelectronics.* 13(3-4). pp. 347-357.
21. Katz, E. 1990. A Chemically Modified Electrode Capable of Spontaneous Immobilization of Amino Compounds due to is Functionalization with Succinimidyl Groups. *J. Electroanal. Chem.* 291. pp. 257-260.
22. Grubor, N.; Shinar, R.; Jankowiak, R. et. al. 2004. Novel Biosensor Chip for Simultaneous Detection of DNA-Carcinogen Adducts with Low-Temperature Fluorescence. *Biosensors and Bioelectronics.* 19. pp. 547-556.
23. Agbasi-Porter, C.; Ryman-Rasmussen, J.; Franzen, S.; Feldheim, D. 2006. Transcription Inhibition Using Oligonucleotide-Modified Gold Nanoparticles. *Bioconjugate Chem.* 17. pp. 1178-1183.
24. Schmid, A.; Stanca; S. Thakur; et. al. 2006. Site-Directed Antibody Immobilization on Gold Substrated for Surface Plasmon Resonance Sensors. *Sensors and Actuators.* 113. pp. 297-303.
25. Jin, W.; Bier, F; Wollengaberg, U; Scheller, F. 1995. Construction and Characterisation of a Multi-Layer Enzyme Electrode: Covalent Binding of Quinoprotein Glucose Dehydrogenase onto Gold Electrodes. *Biosensors and Bioelectronics.* 10. pp. 823-829.

26. Gomes, M.; Duarte, A.; Oliveira, J. 1995. Comparison of Two Methods for coating Piezoelectric Crystals. *Anal. Chim. Acta.* 300. pp. 329-334.
27. Chechik, V.; Crooks, R.; Stirling, C. 2000, Reactions and Reactivity in Self-Assembled Monolayers. *Adv. Mater.* 12. pp. 1161.
28. Tam-Chang, S.; Biebuyck, H.; Whitesides, G.; et. al. 1995. Self-Assembled Monolayers on Gold Generated from Alkanethiols with the Structure $\text{RNHCOOCH}_2\text{SH}$. *Langmuir.* 11. pp. 4371.
29. Lomant, A.; Fairbanks, G. 1976. Chemical Probes of Extended Biological Structures: Synthesis and Properties of the Cleavable Crosslinking Reagent [^{35}S]dithio-bis(succinimidylpropionate). *J. Mol. Biol.* 104. pp. 243-261
30. Wagner, P.; Hegner, M.; Kernen, P.; Zaugg, F.; Semenza, G. 1996. Covalent Immobilization of Native Biomolecules onto Au(1,1,1) via N-Hydroxysuccinimide Ester Functionalized Self-Assembled Monolayers for Scanning Probe Microscopy. *Biophys. J.* 70. pp. 2052-2066.
31. Staros, J. 1982. N-Hydroxysulfosuccinimide Active Esters: Bis(N-hydroxysuccinimide) Esters of two Dicarboxylic Acids are Hydrophilic, Membrane Impermeant, Protein Cross-Linkers. *Biochemistry.* 21. pp. 3950-3955.
32. Staros, J.; Kakkad, B. 1983. Cross-Linking and Chymotryptic Digestion of the Extracytoplasmic Domain of the Anion Exchange Channel in Intact Human Erythrocytes. *J. Memb. Biol.* 74. pp. 247-254.
33. Knoller, S.; et. al. 1989. The Membrane Associate Component of the Amphiphile-Activated, Cytosol-Dependent Superoxide-Forming NADPH oxidase of Macrophages is Identical to Cytochrome b559. *J. Biol. Chem.* 266. pp. 2795-2804.
34. Waugh, S.; et. al. 1989. Isolation of a Proteolytically Derived Domain of the Insulin Receptor Containing the Major Site of Cross-Linking/Binding. *Biochem.* 28. pp. 3448-3455.
35. Duhachek, S.; Kenseth, J.; Casale, G.; et. al. 2000. monoclonal Antibody-Gold Biosensor Chips for Detection of Depurinating Carcinogen-DNA Adducts by Fluorescence Line-Narrowing Spectroscopy. *Anal. Chem.* 72. pp. 3709-3716.
36. Wang, J.; Kenseth, J.; Jones, V.; et. al. 1997. SFM Tip-Assisted Hydrolysis of a Dithiobis(succinimido undecanoate) Monolayer Chemisorbed on a Au(1,1,1) Surface. *J. Am. Chem. Soc.* 119. pp. 12796-12799.

37. Dammer, U.; Hegner, M.; Anselmetti, D.; et. al. 1996. Specific Antigen/Antibody Interactions Measured by Force Microscopy. *Biophys. J.* 70. pp. 1233-1240.
38. Dammer, U.; Popescu, O.; Wagner, P.; et. al. 1995. Quantification of the Intermolecular Binding Strength for a Cell Adhesion Proteoglycan by Scanning Force Microscopy. *Science*. 267. pp. 1173-1175.
39. Lahiri, J.; Isaacs, L.; Tien, J.; Whitesides, G. 1999. A Strategy for the Generation of Surfaces Presenting Ligands for Studies of Binding Based on an Active Ester as a Common Reactive Intermediate: A Surface Plasmon Resonance Study. *Anal. Chem.* 71. pp. 777-790.
40. Peelen, D.; Smith, L. 2005. Immobilization of Amine-Modified Oligonucleotides on Aldehyde-Terminated Alkanethiol Monolayers on Gold. *Langmuir*. 21. pp. 266-271.
41. Hoffmann, E.; Stroobant, V. 2002. Mass Spectrometry Principles and Applications. West Sussex, England. Wiley.
42. Mouradian, S.; Nelson, C.; Smith, L. 1996. A Self-Assembled Matrix Monolayer for UV-MALDI Mass Spectrometry. *J. Am. Chem. Soc.* 118. pp. 8639-8645.
43. Jaakkola, L.; Peuralahti, J.; Hakala, H.; et. al. 2005. Solid-Phase synthesis of Oligonucleotides Labeled with Luminescent Lanthanide(III) Chelates. *Bioconjugate Chem.* 16, pp. 700-709.
44. Smith, Glenn J.; Sosnick, T.; Scherer, N.; et. al. 2004. Efficient Fluorescence Labeling of a Large RNA through Oligonucleotide Hybridization. *RNA*. 11(2), pp. 1-6.
45. McLean, J.; Stumpo, K.; Russel, D. 2005. Size-Selected (2-10 nm) Gold Nanoparticles of Matrix Assisted Laser Desorption Ionization of Peptides. *J. Am. Chem. Soc.* 127. pp. 5304-5305.
46. Cumberland, S.; Strouse, G. 2002. Analysis of the Nature of Oxyanion Adsorption on Gold Nanomaterial Surfaces. *Langmuir*. 18. pp. 268-276
47. Williams, D.; Fleming, I. 1987. Spectroscopic Methods in Organic Chemistry. McGraw Hill. London.
48. Boyer, R. Modern Experimental Biochemistry. 2000. Boston. Addison Wesley Longman.
49. Robyt, J.; White, B. 1990. Biochemical Techniques Theory and Practice. Prospect Heights, IL. Waveland Press, Inc.

50. Alvisatos, Paul. 2004. The use of Nanocrystals in Biological Detection. *Nature Biotechnology*. 22. pp. 47-52.
51. Sawyer, D.; Heineman, W.; Beebe, J. 1984. Chemistry Experiments for Instrumental Methods. New York. John Wiley & Sons, Inc.
52. Kreibig, U.; Vollmer, M. 1995. Optical Properties of Metal Clusters. Berlin: Springer Verlag.
53. Peterlinz, K.; Georgiadis, R. 1997. Observation of Hybridization and Dehybridization of Thiol-Tethered DNA Using Two-Color Surface Plasmon Resonance Spectroscopy. *J. Am. Chem. Soc.* 119. pp. 3401-3402.
54. Raether, H. 1988. Surface Plasmons, Springer Tracts in Modern Physics; Berlin. Springer Verlag.
55. Peterson, A.; Wolf, L.; Georgiadis, R. 2002. Hybridization of Mismatched or Partially Matched DNA at Surfaces. *J. Am. Chem. Soc.* 124. pp. 14601-14607.
56. Wiedlich, T.; Lindsay, S.; Rupprecht, A. 1987. The Optical Properties of Lithium and Sodium DNA Films. *Biopolymers*. 26. pp. 439-453.
57. Tinland, B.; Pluen, A. et. al. 1997. Persistence Length of Single-Stranded DNA. *Macromolecules*. 30. pp. 5763.
58. Castelino, Kenneth; Kannan, Balaji; Majumdar, Arun. 2005. Characterization of Grafting Density and Binding Efficiency of DNA and Proteins of Gold Surfaces. *Langmuir*. 21. pp. 1956-1961.
59. Joshi, Hrushikesh; Shirude, Pravin; et. al. 2004. Isothermal Titration Calorimetry Studies on the binding of Amino Acids to Gold Nanoparticles. *J. Phys. Chem.* 108. pp. 11535-115.
60. Cumberland, S.; Strouse, G. 2002. Analysis of the Nature of Oxyanion Adsorption on Gold Nanomaterial Surfaces. *Langmuir*. pp. 269-276.
61. Frey, B.; Corn, R. 1996. Covalent Attachment and Derivatization of Poly(L-lysine) Monolayers on Gold Surfaces as Characterized by Polarization-Modulation FT-IR Spectroscopy. *Anal. Chem.* 68. pp. 3187-3193.
62. Lin-Vien, D.; Colthup, N.; Fateley, W.; Grassetti, J. 1991. The Handbook of Infrared and Raman Characteristic Frequencies of Organic Molecules. Boston. Academic Press.

63. Hasan, M.; Bethell, D.; Brust, M. 2002. The Fate of Sulfur-Bound Hydrogen on Formation of Self-Assembled Thiol Monolayers on Gold: ^1H NMR Spectroscopic Evidence from Solutions of Gold Clusters. *J. Am. Chem. Soc.* 124(7). pp. 1132-1133.
64. Luedtke, W.; Landman, U. 1998. Structure and Thermodynamics of Self-Assembled Monolayers on Gold Nanocrystallites. *J. Phys. Chem.* 102. pp. 6566-6572.
65. Bourg, M.; Badia, A.; Lennox, R. 2000. Gold-Sulfur Bonding in 2D and 3D Self-Assembled Monolayers; XPS Characterization. *J. Phys. Chem.* 104. pp. 6562-6567.
66. Weber, K.; Osborn, M. 1969. The Reliability of Molecular Weight Determinations by Dodecyl Sulfate-Polyacrylamide Gels. *J. Biol. Chem.* 244. pp. 4406.
67. Nelson, B.; Grimsrud, T.; Corn, R.; et. al. 2001. Surface Plasmon Resonance Imaging Measurements of DNA and RNA Hybridization Adsorption onto DNA Microarrays. *Anal. Chem.* 73. pp. 1-7.
68. Yang, W.; Chen, M.; Knoll, W.; et. al. 2002. Synthesis of Hexanedithiolate/Decanethiolate Mixed Monolayer Protected Gold Clusters and Scanning Tunneling Microscope Induced Patterning on the Clusters/Au(1,1,1) Surface. *Langmuir*. 18. pp. 4124-4130.
69. Simard, J.; Briggs, C.; Boal, A. Rotello, V. 2000. Formation and pH-Controlled Assembly of Amphiphilic Gold Nanoparticles. *Chem. Commun.* pp. 1943-1944.

VITA

Kevin Francis earned his bachelors degree from the University of Missouri-Columbia before starting his professional career in 1995. Initial work was in the field of environmental chemistry serving as a Chemist/Project Manager in the analysis of soil, water and air samples for trace levels of inorganic and organic analytes deemed as pollutants by the EPA. Following his analytical work was research and development of sensors for chemical and biological warfare agents beginning in 1999. This work included the development of several BioMEMS devices such as a microfluidic FRET immunoassay chip for optical interrogation of biowarfare agents; a MEMS ELISA biochip that encompassed a dilution network, valves and mixers; TNT/DNT vapor biosensor for the detection of unexploded ordinance; hydrogen based MEMS PEM fuel cell; a microfluidic PCR chip; and the development of a paramagnetic bead based immunosensor for the detection of biological threats in water supplies. In September of 2005, his focus shifted towards the goal of Master of Science at Texas State University-San Marcos. Current work involves the development of an automated, multi-analyte paramagnetic bead based immunosensor utilizing quantum dot technology.

Permanent Address: 145 High Grove

Cedar Creek, TX 78612

This thesis was composed by Kevin Francis.